The Crab Nebula: An Astrophysical Chimera

J. Jeff Hester

School of Earth & Space Exploration, Arizona State University, Tempe, Arizona 85287; email: jhester@asu.edu

Annu. Rev. Astron. Astrophys. 2008. 46:127–55

First published online as a Review in Advance on May 19, 2008

The *Annual Review of Astronomy and Astrophysics* is online at astro.annualreviews.org

This article's doi: 10.1146/annurev.astro.45.051806.110608

0066-4146/08/0922-0127$20.00

Key Words

pulsar wind nebulae, supernova remnants, historical supernovae

Abstract

The Crab Nebula, henceforth the Crab, the remnant of the historical supernova of 1054 AD, has long been of intense interest. The pulsar at the center of the Crab has a spin-down luminosity $\sim 10^5$ times that of the Sun. The outer nebula holds several solar masses of material ejected by the explosion. Between the two lies the trapped pulsar wind, visible as synchrotron radiation at radio wavelengths through X-ray wavelengths. Recent observations with the *Hubble Space Telescope*, the *Chandra X-ray Observatory*, and a host of other instruments have provided a wealth of information about the extraordinary structure and dynamics of the Crab. Understanding those data requires thinking of the Crab not in terms of its individual components, but instead as a single interconnected physical system formed as the axisymmetrical wind from the pulsar pushes its way outward through a larger freely expanding supernova remnant.

1. INTRODUCTION

The Crab Nebula is the remnant of a supernova explosion witnessed by Chinese astrologers on July 4, 1054 AD. Even at a distance of ~2 kpc (Trimble 1968), the Chinese astronomer Wang Yei-te reported that the "guest star" was visible during the daytime for three weeks, and was visible at night for 22 months (Clark & Stephenson 1977). Following its rediscovery in 1731 by the English astronomer John Bevis, the Crab Nebula was observed in 1758 by Charles Messier and became the first object in his famous catalog of nebulous noncometary objects. The Crab was given its name circa 1850 by William Parsons, third Earl of Rosse, who observed the appearance through his 72-inch reflecting telescope. Lundmark (1921) suggested a connection between the Crab Nebula and the event of 1054 AD, but it was not until 1942 that Duyvendak (1942) and Mayall & Oort (1942) presented complete studies of modern observations of the expanding nebula and of the early Chinese records. It was this work that established unambiguously that the Crab is the remnant of SN1054.

Today the Crab Nebula (**Figure 1**) is perhaps the most observed object in the sky beyond our own solar system and is related to almost every branch of astrophysics. This review of the Crab is timely given the amount of recent observational work on the object using facilities such as the *Hubble Space Telescope* (HST) (Hester et al. 1995, 1996; Blair et al. 1997; Sankrit & Hester 1997; Hester 1998; Sankrit et al. 1998; Loll et al. 2007; Hester, 2007), the *Chandra X-ray Observatory* (*Chandra*) (Weisskopf et al. 2000; Hester et al. 2002; Mori et al. 2004; Seward, Gorenstein & Smith 2006; Seward, Tucker & Fesen 2006) the *Spitzer Space Telescope* (*Spitzer*) (Temim et al. 2006), and the Very Large Array (VLA) (Frail et al. 1995; Bietenholz, Frail & Hester 2001; Bietenholz et al. 2004). The current importance of the Crab Nebula to astrophysics stems from the quality of these observations, because they allow perhaps a more complete and detailed comparison between theory and observations than is possible with any other nonstellar astrophysical object.

The volume of the literature on the Crab Nebula is large. An ADS abstract search on the name turns up over 5000 references. A comprehensive review of this wealth of literature is virtually impossible and would do little to clarify understanding of this remarkable object. (For that reason references in this review are often representative rather than exhaustive. I apologize in advance to those whose excellent work may not be cited.) As a consequence of the wealth of observational and theoretical work on the Crab, what is often missing is synthesis. Observers and theorists who are working on one aspect of the Crab or related topics may be unaware or unfamiliar with aspects of the remnant that are relevant to their studies. With this audience largely in mind, this review approaches the literature with an eye toward forming such a synthesis. It offers an overall physical description of the Crab, which, even where it turns out to be incomplete or incorrect, might still provide a common physical context in which current and future work can be discussed. That picture will not be of a freely expanding remnant of a possibly underluminous explosion, as is often proposed. Instead, this review concludes that the Crab is best thought of as a pulsar wind nebula (PWN) confined by and pushing out into a much larger, freely expanding remnant, as first proposed by Chevalier (1977). It is likely that this larger but almost unseen remnant contains most of the mass and kinetic energy of the explosion. Were it not for the spin-down luminosity of the pulsar, the pressure of the PWN that has compressed some of the ejecta into dense filaments, and the synchrotron radiation from the PWN that photoionizes that ejecta, the Crab Nebula might be known today by little more than obscure historical references to an especially bright "guest star" observed in 1054 AD.

To avoid confusion it is worth prefacing a review of the Crab with a few notes on the nomenclature that has grown up around the object. Moving from the inside out, the Crab consists of the Crab pulsar, the Crab synchrotron nebula, a bright expanding shell of thermal gas, and a larger

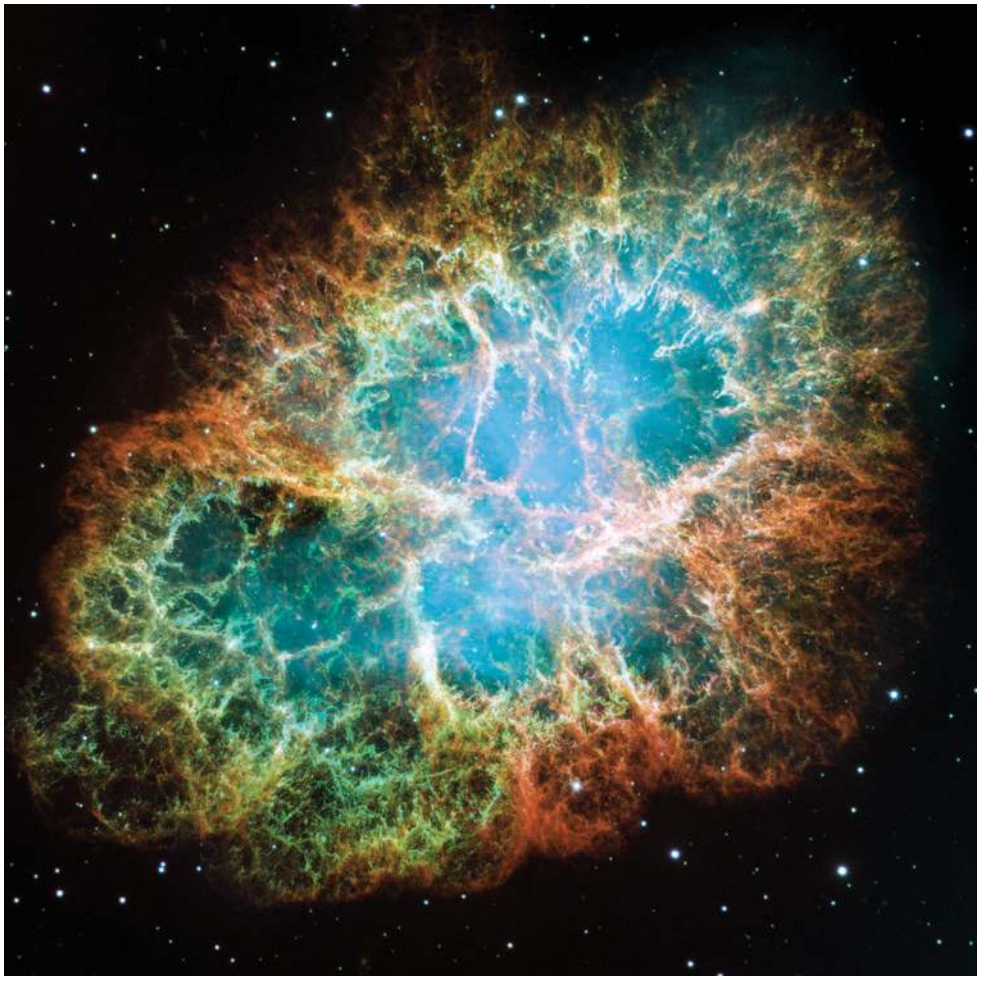

Figure 1

A composite *Hubble Space Telescope* image of the Crab Nebula. Thermal filaments composed of ejecta from the explosion appear around the outer part of the nebula. [O III] λ5007 is shown in red, [S II]λλ6717,6731 in green, and [O I]λ6300 in blue. Note that much of the structure breaks up into inward pointing fingers of emission. Note also the increasing ionization moving outward and the scalloped appearance of the nebula. The visible synchrotron nebula filling the interior of the remnant is shown in blue. The synchrotron nebula is bounded and confined by the thermal ejecta. Note the presence of a red [O III] "skin" around the SE portion of the remnant, which is interpreted as emission behind a shock driven by the pressure of the synchrotron nebula into a larger, freely expanding remnant surrounding the Crab.

very faint freely expanding supernova remnant. By convention, features in the synchrotron nebula are referred to as wisps. Structures seen in the light of emission lines from thermal gas are referred to as filaments. The wind shock is located at the interface between the wind and the synchrotron nebula. There is a second shock at the outer boundary of the synchrotron nebula driven by the pressure of the synchrotron nebula into surrounding thermal gas. The synchrotron nebula and thermal filaments lie within a larger freely expanding supernova remnant. All of these components have been observed either directly or indirectly. An as yet unseen outer shock presumably lies well beyond the visible boundary of the Crab at the leading edge of the expanding cloud of ejecta.

2. THE CRAB CONSISTS OF FOUR OBSERVABLE COMPONENTS

2.1. The Crab Pulsar Powers the Nebula

The Crab Nebula consists of four observable components. At the center of the Crab lies the Crab pulsar. Since its discovery at radio wavelengths (Staelin & Reifenstein 1968, Comella et al. 1969),

the Crab pulsar has been studied intensively in all wavelength regimes from gamma rays to radio. It was the first pulsar to be observed at visible wavelengths (Cocke, Disney & Taylor 1969).

The Crab pulsar has a period of 33 ms, and $\dot{P} = 4.21 \times 10^{-13}$. Assuming a uniform sphere with a radius of 10 km and a mass of 1.4 $M_\odot$, the moment of inertia of the pulsar is $I = 1.1 \times 10^{45}$ g cm^2. The pulsar then has a spin-down luminosity of $L_{spin} = 4\pi^2 I \frac{\dot{P}}{P^3} \cong 5 \times 10^{38}$ erg s^{-1}, or 130,000 $L_\odot$. Using a braking index $n = 2.51$ (Lyne, Pritchard, & Smith 1988), Bejger & Haensel 2003 estimate that the pulsar was born with a period of ~19 ms, so it has lost $\sim 3.6 \times 10^{49}$ ergs since its birth. This corresponds to an average luminosity of $\sim 1.2 \times 10^{39}$ergs s^{-1} over the lifetime of the remnant, or about twice the current value. Although a small fraction of this energy goes into pulsed emission, the majority of the pulsar's spin-down luminosity is carried away by some combination of magnetic dipole radiation and an ultrarelativistic wind. Kennel & Coroniti (1984a) point to the high efficiency with which this energy is converted into synchrotron emission in the Crab. Since this work, it has typically been assumed that the pulsar's spin-down luminosity is carried for the most part by a highly magnetized pair plasma, perhaps with some admixture of ions from the surface of the neutron star itself (Gallant & Arons 1994). (This review makes the same assumption throughout.) This is the source of the energy that powers the Crab.

2.2. The Shocked Pulsar Wind Fills the Crab Synchrotron Nebula

The pulsar's ultrarelativistic wind is confined by the thermal ejecta from the explosion into which it is expanding. Little or no synchrotron emission is seen from the wind in the volume immediately surrounding the pulsar (Schmidt, Angel & Beaver 1979), indicating that the wind itself is not luminous. The transition from this cold fast wind (dominated by the kinetic energy of the flow) to the hot plasma that fills the nebula occurs in a shock. Momentum balance between the wind and the synchrotron nebula suggests that the shock should be located about 3×10^{17} cm from the pulsar (Rees & Gunn 1974, Kennel & Coroniti 1984a), and it is often pointed out that this is roughly the projected distance between the pulsar and the wisps observed by Scargle (1969). As discussed below, more recent imaging of the Crab synchrotron nebula shows that this picture is overly simplistic and that the pulsar wind is far from spherically symmetrical. Even so, there are a number of quasi-stationary features (e.g., the X-ray ring from Weisskopf et al. 2000 and the sprite and halo from Hester et al. 2002) that are plausibly identified with the shock. In no direction does the energy flow from the pulsar appear unconfined.

In the simple model, the wind shock thermalizes flow energy, accelerating electrons and positrons to energies as high as $\sim 10^4$ TeV. It is this magnetized relativistic plasma that gives off the synchrotron emission that we see. Alfvén & Herlofson (1950) were the first to suggest synchrotron emission as a mechanism for bright radio emission from radio stars. The Crab synchrotron nebula was the first confirmed astrophysical source of synchrotron radiation (Shklovsky 1953, Dombrovsky 1954) and is the defining member of the class of center-filled flat spectrum supernova remnants called plerions (Weiler & Panagia 1978). Although the term plerion remains a morphological designation, most plerions are now identified with PWN. The Crab synchrotron nebula fills a roughly ellipsoidal volume with a major axis of 4.4 pc and a minor axis of 2.9 pc, tilted into the plane of the sky by 30° (Lawrence et al. 1995, Loll et al. 2007), and fills a volume of $\sim 10^{57}$ cm^3 or ~30 pc^3.

The Crab Nebula is remarkably efficient at converting the energy of the shocked pulsar wind into synchrotron emission. The synchrotron emission from the Crab Nebula has an integrated luminosity of $\sim 1.3 \times 10^{38}$ ergs s^{-1}, or about 26% of the 5×10^{38} ergs s^{-1} currently being injected into the nebula by the pulsar. A comparable fraction of the energy lost by the pulsar has gone into PV (pressure-volume) work done on the filaments, leaving perhaps half of the energy lost by the

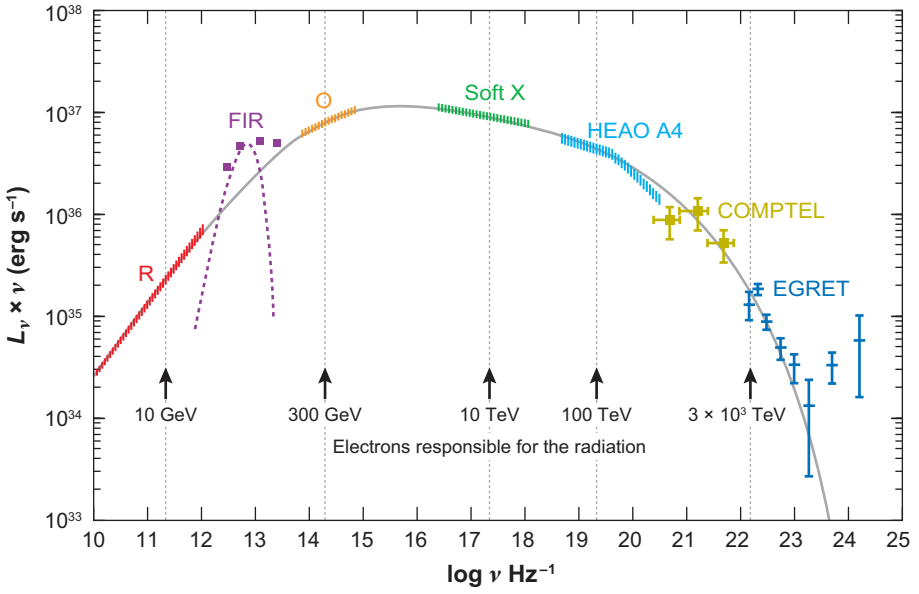

Figure 2

The integrated spectrum of the Crab synchrotron nebula, from Atoyan & Aharonian (1996), assembled from sources cited in that paper. The electron energies shown correspond to peak synchrotron emission assuming a magnetic field of 300 μG. Most of the emission from the Crab is emitted between the optical and X-ray bands. The highest energy γ-rays are due to inverse Compton radiation.

pulsar ($\sim 1.8 \times 10^{49}$ergs) still resident within the synchrotron nebula. Averaged over the volume of the synchrotron nebula, this energy density corresponds to a pressure of $\sim 7.2 \times 10^{-9}$ dyne cm^{-2}, very close to the canonical value assuming equipartition and B $\sim$ 300 μG (Trimble 1968).

The overall spectrum of the Crab Nebula peaks in the range between 10^{14}–10^{18} Hz in the optical through the X-ray part of the spectrum (see **Figure 2**, from Atoyan & Aharonian 1996). Assuming a magnetic field of 300 μG, this radiation is associated with emission from electrons with energies between a few hundred GeV and a few tens of TeV. The very highest energy emission from the Crab above frequencies of $\sim 10^{23}$ Hz is thought to be due to inverse Compton radiation (Atoyan & Aharonian 1996). The bump around 10^{13} Hz in the far infrared part of the spectrum is the result of thermal emission from dust in the nebula. This dust, which condensed from material ejected in the explosion, is heated to a temperature of about 80 K (Marsden et al. 1984).

Figure 3 shows a color composite image of the Crab synchrotron nebula. An X-ray image of the Crab obtained with *Chandra* is shown in blue. An optical continuum image is shown in green. Red shows a radio image of the Crab obtained with the VLA. The first thing that is immediately apparent in these images is the difference in spatial extent of the Crab synchrotron nebula when viewed at different wavelengths. The nebula is smallest in size when viewed at high energies, and grows progressively larger when viewed at lower energies. This basic trend is relatively easy to understand. High-energy particles injected into the nebula at the wind shock experience both synchrotron burn off and energy loss owing to adiabatic expansion as they move outward through the nebula. Even so, faint X rays are still seen close to the boundary of the nebula (Hester et al. 1995; Seward, Tucker & Fesen 2006), indicating that the real situation is more complex.

The synchrotron nebula shows a wealth of fine-scale structure that can be extraordinarily dynamic, varying appreciably on timescales of days. The standard nomenclature for these features comes from Scargle (1969), who identified a number of arcuate features or wisps located along and generally perpendicular to a line going from the SE to the NW through the pulsar. (By convention, features in the Crab synchrotron nebula are referred to as wisps, while the term filament is reserved

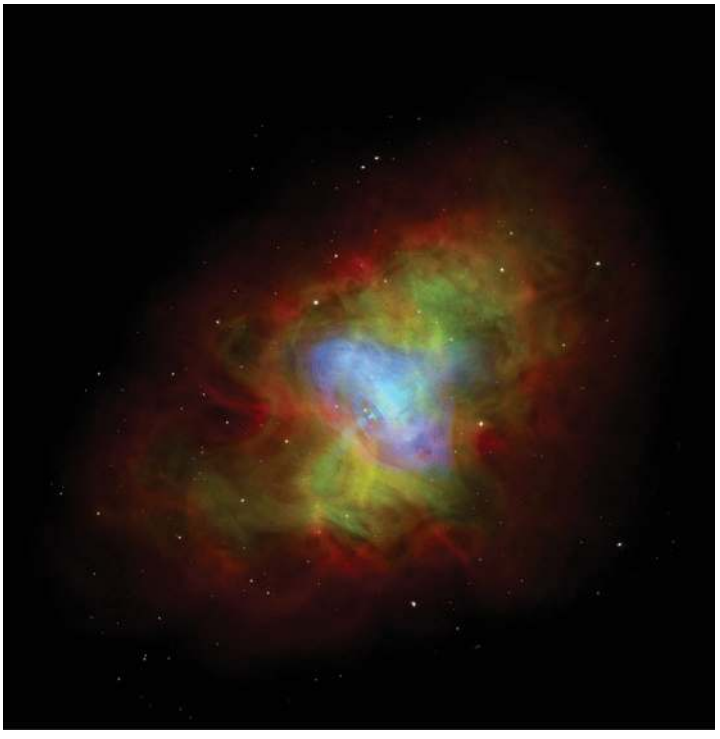

Figure 3

Color composite of the Crab synchrotron nebula showing a *Chandra* X-ray image in blue, a visible light mosaic taken with HST in green, and a VLA radio image in red. The pulsar is seen as the bright blue point source at the center of the image. Note the axisymmetry of the nebula, which is most apparent from the X-ray torus and jets. Emission from high-energy electrons is brightest near the center of the nebula, close to where they are injected. Moving outward through the nebula, the spectrum becomes softer owing to adiabatic and radiative losses. For the most part, only low-energy radio-emitting electrons survive to the edge of the nebula.

for features seen in thermal emission from ejecta.) High spatial resolution (~0".5) ground-based optical imaging showed that the prominent wisps are only the most obvious of the fine structure present in the Crab (van den Bergh & Pritchet 1989). The resolution of HST images (Hester et al. 1995) nears the scale of the Larmor radius of the most energetic electrons present.

Serious efforts to model the Crab synchrotron nebula go back to the work of Rees & Gunn (1974). The standard set of models for the Crab to which subsequent work is typically referred is the work of Kennel & Coroniti (1984a,b), who calculate spherically symmetrical models of the expansion of a pulsar wind that is confined by a surrounding thermal shell. These models are constrained by the need to match the outer boundary condition set by the observed expansion speed of the surrounding thermal ejecta, as well as the inferred location of the wind shock. The adjustable parameter in these models is the ratio immediately upstream of the shock of the magnetic energy flux to the energy flux carried by particles, generally written as σ. As demonstrated in Kennel & Coroniti's models, σ must be relatively low in order for the wind to shock close to the pulsar. Theory suggests that pulsar winds are born as magnetically dominated high σ flows. The conversion of a high σ flow to a low σ flow is referred to as the "σ problem" and remains a field of active research. The general problem of pulsar winds and PWN has been discussed recently in a number of reviews including those of Arons (2008) and Gaensler & Slane (2006), so further discussion here will focus on the specific properties of the PWN in the Crab.

2.3. Thermal Filaments Form a Cage Around the Synchrotron Nebula

The third observable component of the Crab Nebula is the network of thermal filaments that are composed of ejecta from the supernova, possibly mixed with some material from the pre-supernova

wind (Fesen, Margin & Shull 1992). The filaments form an expanding cage that confines the synchrotron nebula. Observed expansion velocities range from about ∼700–1800 km s^{-1}, with 1500 km s^{-1} being a characteristic value at the edge of the nebula (Clark et al. 1983). Comparison of these values with observed proper motions gives the estimated distance to the Crab of about 2 kpc. These expansion velocities set boundary conditions for models of the structure of the PWN. The filaments show line emission covering a wide range of ionization states, ranging from H_2 (Graham, Wright & Longmore 1990) up to and including such high ionization lines as CIV λ1549 (Blair et al. 1992) and [NeV] λ3426 (Davidson 1979). Helium lines are especially prominent in the Crab, consistent with depletion of most of the hydrogen in the ejecta by nuclear burning in the progenitor (Miller 1978, MacAlpine et al. 2007). Most (but not all) of the emission from the filaments is the result of photoionization by the hard continuum from the synchrotron nebula. Filaments also contain dust, which can be seen in extinction against the background of the synchrotron nebula (Sankrit et al. 1998), as well as in a bump in the spectrum in the thermal infrared (Marsden et al. 1984).

2.4. There is Freely Expanding Ejecta Beyond the Easily Visible Crab

The existence of these three components and the basic aspects of the relationship among them have been more or less understood since the 1970s. The last major review of the Crab in the literature was the review by Davidson & Fesen (1985), who discuss its fundamental properties. There is a fourth, more recently appreciated, component of the Crab Nebula consisting of freely expanding ejecta from the supernova located outside the easily visible edge of the nebula. This component of the Crab has been an important part of many theoretical models of the Crab for three decades and is crucial to a complete physical description of the object, but only recently have observations provided direct evidence of its existence.

3. THE CRAB NEBULA THAT WE SEE IS NOT A FREE EXPANSION SUPERNOVA REMNANT

The Crab Nebula was the first established example of the remnant of a historical supernova and once constituted the textbook example of a free expansion supernova remnant in which ejecta from the explosion has yet to be slowed significantly by swept-up interstellar gas. There have always been problems with this description, however. Spectroscopic studies of the filaments in the Crab consistently give ejecta masses of order 2–5 $M_\odot$ (Fesen, Shull & Hurford 1997), less than the minimum mass that should be ejected by a core collapse supernova. The radial velocity measurements show that the filaments are expanding at velocities less than ∼1500 km sec^{-1} (Clark et al. 1983), significantly less than the velocities of 5000–10,000 km sec^{-1} seen in the spectra of supernovae and in young remnants such as Cas A. Together, these give a kinetic energy of perhaps 3×10^{49} ergs, which is a factor of 30 less than the canonical 10^{51} ergs seen in the ejecta of core collapse supernovae. It has been suggested that SN1054 was an atypical low-energy explosion (e.g., Frail et al. 1995), but the light curve of the supernova reconstructed from detailed historical records seems to be that of a normal Type II event (Chevalier 1977).

Perhaps the most obvious flaw in the description of the Crab as a free expansion SNR is the fact that it is not freely expanding. Mayall & Oort (1942) noted that the expansion age of the Crab appeared to be about 800 years, or about 90 years less than the time since the explosion, and realized that something must be causing the expansion to accelerate. More recent studies of the expansion of the Crab give convergence dates that vary, but generally lie within the range of 1120 AD to 1233 AD (Trimble 1968, Wyckoff & Murray 1977, Bietenholz et al. 1991), with later

values inferred for features closer to the edge of the nebula. These values imply that ejecta are moving ~100–300 km s^{-1} faster than the free expansion velocity. This accelerated expansion is the result of the pressure of the confined synchrotron nebula acting on the thermal ejecta (Trimble & Woltjer 1971). Using characteristic values of 2 $M_\odot$ of thermal ejecta and acceleration from 1350 km s^{-1} to 1500 km s^{-1} requires that $\sim 9 \times 10^{48}$ ergs, or ~25% of the total energy lost by the pulsar has gone into PV work done on thermal ejecta. This is comparable to the fraction of the spin-down luminosity that goes into synchrotron emission.

3.1. Filament Structure is Shaped by Rayleigh-Taylor Instabilities

High-resolution images of the Crab taken in the light of several emission lines, in particular images taken with HST, show that the filaments have a far more complex structure than previously assumed (Hester et al. 1996, Blair et al. 1997, Sankrit et al. 1998, Loll et al. 2007). These data show that the classical filaments in the Crab actually break up into many smaller structures. These structures often exhibit a head-to-tail or finger-like structure pointing inward into the center of the nebula. Fingers are typically less than an arcsecond across, range in length from less than an arcsecond up to about 20", and are usually attached to their neighbors by arc-like bridges of emission. This bubble-and-spike morphology of the filaments has been interpreted as the result of Rayleigh-Taylor (R-T) instabilities acting at the interface between the confined synchrotron nebula and thermal ejecta. Hester et al. (1996) found that the observed wavelength of the instability, the local acceleration at the interface, the density of the gas in the filaments, and the magnetic field inferred from the synchrotron nebula satisfy the relationship for magnetic R-T instabilities from Chandrasekhar (1961). (Briefly, in a magnetic R-T instability, also known as a Kruskal-Schwarzschild instability, the magnetic tension in a field parallel to the interface can suppress short-wavelength modes.)

It has long been understood that the interface between the light synchrotron plasma and denser thermal ejecta is subject to R-T instabilities (see Davidson & Fesen 1985), and this explanation had been suggested for the Crab prior to the HST observations (e.g., Chevalier & Gull 1975; Bandiera, Pacini & Salvati 1983). Following the HST observations, there has been a good deal of subsequent theoretical work examining the behavior of this instability (e.g., Jun 1998, Bucciantini et al. 2004). These simulations produce structures that bear a strong resemblance to observations of the filaments in the Crab. In the simulations by Jun (1998), the density of the gas in the high-density heads of R-T fingers is about 10 times the density in other regions of thermal gas, even ignoring the effects of radiative cooling, with 60–75% of the shocked mass concentrated in the R-T fingers. Stone & Gardiner (2007) discuss the behavior of the instability in three dimensions and find that the magnetic field plays a key role in the development of the instability. Specifically, even weak magnetic fields can be effective in suppressing secondary instabilities, reducing mixing between the two fluids and allowing R-T fingers to grow more rapidly and to larger sizes than often assumed. Hester et al. (1996) suggested that this mechanism along with differences in field strength in the thermal filaments might account for differences in the filament morphologies. Detailed application of this theory to the Crab is complicated, however, by effects including radiative cooling and differences in the field strength between the thermal and synchrotron plasmas.

One important complication in applying the theory of magnetic R-T instabilities to the Crab is the fact that a uniform magnetic field can only stabilize the interface along the direction of the field. Stone & Gardiner (2007) find, however, that if the field direction changes by large angles near the interface, magnetic R-T instabilities can suppress short-wavelength modes in all directions. Polarization observations of the Crab (Hester 2007; see below) show that the synchrotron nebula is layered, with field alignment changing on scales of a few times 10^{16} cm. The resulting magnetic

structure might be visualized as much like the layers of belting in a radial tire and might stabilize the interface in all directions, much as Stone & Gardiner suggest.

3.2. A Freely Expanding Remnant Surrounds the Visible Crab

As noted above, only $\sim 10^{49.5}$ ergs can be accounted for in the kinetic energy of the observed ejecta. Chevalier (1977) was among the first to suggest that most of the mass and kinetic energy of the Crab is contained in an extended but (at that time) unobserved freely expanding remnant. In this view, the outer edge of the synchrotron nebula and the corresponding outer edge of the thermal filaments (i.e., the visible extent of the nebula) traces the location of a shock that is driven by the confined synchrotron nebula into the surrounding freely expanding remnant. (The shock at the visible edge of the Crab should not be confused with the unseen outer shock driven in advance of the ejecta itself. Assuming ejecta velocities typical of core collapse supernovae, the outer shock should be at several times the radius of the visible remnant.)

There have been a number of searches for evidence of the freely expanding remnant that surrounds the visible Crab. Murdin & Clark (1981) and Murdin (1995) report direct detection of a halo around the Crab, but observations with better detection limits have failed to confirm these claims (e.g., Fesen 1997; Fesen, Shull & Hurford 1997). It is not surprising that a halo around the Crab is difficult to detect. Sankrit & Hester (1997) found that it was possible for an extended freely expanding remnant around the Crab to have a mass $>5\ M_\odot$ and kinetic energy $>5 \times 10^{50}$ ergs without violating the formal limit on Hα emission measure (4.2 cm^{-6} pc) from Fesen, Shull & Hurford (1997). Detection of this component is made even more difficult by its broad ($\sim$1500 km sec^{-1}) line width.

The existence of a freely expanding remnant surrounding the visible Crab can, however, be inferred from the existence of the shock driven by the synchrotron nebula. If such a shock is present, then there must be a suitable medium into which it is being driven. In their theoretical model of the evolution of the Crab, Chevalier & Fransson (1992) predicted that this shock velocity should be about 230 km s^{-1}. At that velocity, the shock would be nonradiative and difficult to detect. Bietenholz et al. (1997) searched for variations in the radio spectral index at the edge of the synchrotron nebula, which might be due to shock acceleration, but found none. The first observational evidence for the shock at the edge of the synchrotron nebula (Hester et al. 1996) was based on the morphology of the R-T fingers seen in HST images of the thermal ejecta. Each R-T finger in these images is connected to its neighbors by thin arcs or bubbles of the sort characteristic of the R-T instability. These bubbles would not be present were there no surrounding medium into which the synchrotron nebula is pushing. Numerical simulations of the expansion of the Crab invariably identify these observed arcs with material from a surrounding freely expanding remnant that has been compressed by the synchrotron-driven shock (Jun 1998, Bucciantini et al. 2004).

The actual unstable interface between the synchrotron nebula and the ejecta is much less conspicuous than the bright filaments themselves. This interface is seen as a thin, faint skin of high-ionization emission that outlines much of the edge of the synchrotron nebula. The first reported detection of what is now understood as the shock at the observed edge of the Crab may be that of Gull & Fesen (1982), who noted that the Crab has a sharp edge when viewed in [O III] emission. Long-slit spectra of the Crab published by Clark et al. (1983) also show that the bright filaments are enclosed by a faint but well-defined component of high-velocity [O III] emission.

Sankrit & Hester (1997) modeled the observed high-ionization skin around the Crab as the cooling region behind the synchrotron-driven shock. They note that observations of the expansion of the Crab give values that range from about 100 km s^{-1} to 285 km s^{-1} faster than free expansion.

Because this is the velocity at which the observed filaments are overtaking freely expanding ejecta, it can be equated with the shock velocity. Assuming a canonical value for the magnetic field of 300 μG, they balance the driving pressure with the ram pressure at the shock, $B^2_{synch}/8\pi = \frac{3}{4}\rho_0 v_s^2$, and find that the density of the ejecta just outside the shock is $\rho/m_H \sim 12.7(v_s/150 \text{ km s}^{-1})^{-2} \text{ cm}^{-3}$. With the driving pressure, shock velocity, and preshock density known, shock models are well constrained. Sankrit & Hester (1997) found that such models correctly predict the brightness of the [O III] skin and can be distinguished from power-law photoionization models for the skin on the basis of the strength of high-ionization emission. For shock velocities greater than about 150 km s^{-1}, shock models predict C IV and [Ne V] emission about a factor of 10 higher than can be accounted for by photoionization models. The values predicted by the shock models are in good agreement with C IV λ1549 *Hopkins Ultraviolet Telescope* (HUT) observations from Blair et al. (1992) and [Ne V] λ3426 observations reported by Davidson (1979). (It should be emphasized that the 1500 km s^{-1} shock that would be driven into stationary ambient gas around the visible Crab would fail to match any of the observed properties at the edge of the visible nebula. Only a shock driven into freely expanding ejecta is allowed by the observations.) The best image of the shock around the edge of the synchrotron nebula is the [Ne V] image shown in **Figure 4**.

The presence of a shock around the edge of the synchrotron nebula implies the existence of a larger freely expanding remnant around the Crab. This larger remnant was finally detected directly by Sollerman et al. (2000), who found C IV λ1550 absorption to be blueshifted in an HST STIS spectrum of the Crab pulsar. The observed feature extends blueward from about −1200 km s^{-1}, the expansion velocity of dense filaments, to about −2500 km s^{-1} before it is lost in noise. Sollerman et al. (2000) put conservative lower limits on the mass and kinetic energy of the extended remnant of $M > 0.3\ M_\odot$ and KE $> 1.5 \times 10^{49}$ ergs, respectively, leaving open the possibility that SN1054 was an underluminous event. They note, however, that the C IV absorption seen in the pulsar spectrum is consistent with $M \sim 8\ M_\odot$ and KE $\sim 10^{51}$ ergs in the freely expanding ejecta, assuming the ejecta density falls off no faster than $\sim r^{-4}$.

3.3. The Crab is Expanding into a Cavity

If there is a freely expanding supernova remnant surrounding the visible Crab, then there must be an outer shock driven into ambient interstellar material by the expanding ejecta. Assuming a maximum ejecta velocity of around 10,000 km s^{-1}, this shock should have a radius of as much as 10 pc, or about seven times the radius of the observed Crab. Despite concerted efforts to find this shock at radio (e.g., Frail et al. 1995) and X-ray (e.g., Mauche & Gorenstein 1989; Predehl & Schmitt 1995; Seward, Gorenstein & Smith 2006) wavelengths, it has not been observed. In this instance, however, absence of evidence should not be taken as evidence of absence.

There have been a number of studies of the interstellar environment of the Crab that show that the remnant is located within a large, low-density void in the H I distribution (Romani et al. 1990; Wallace, Landecker & Taylor 1994; Wallace et al. 1999), roughly 130 pc across. This cavity is thought to have formed as a result of energy input from stellar winds and/or previous supernovae. Frail et al. (1995) point out that for the Crab's ejecta-driven shock to have escaped detection at radio wavelengths the density inside this bubble would have to be very low, or the shock at the outer edge of the ejecta would have to be very inefficient at producing synchrotron emission. A similar conclusion is reached in the X-ray study by Seward, Gorenstein & Smith (2006). Even so, these researchers acknowledge that the shock from a 10^{51} erg explosion of an 8–13 $M_\odot$ progenitor would be undetectable, so long as the ejecta are warm (10^4–10^5 K) and the cavity tenuous ($n \sim 0.01 \text{ cm}^{-3}$). They then assert that this is unlikely. That assertion deserves scrutiny.

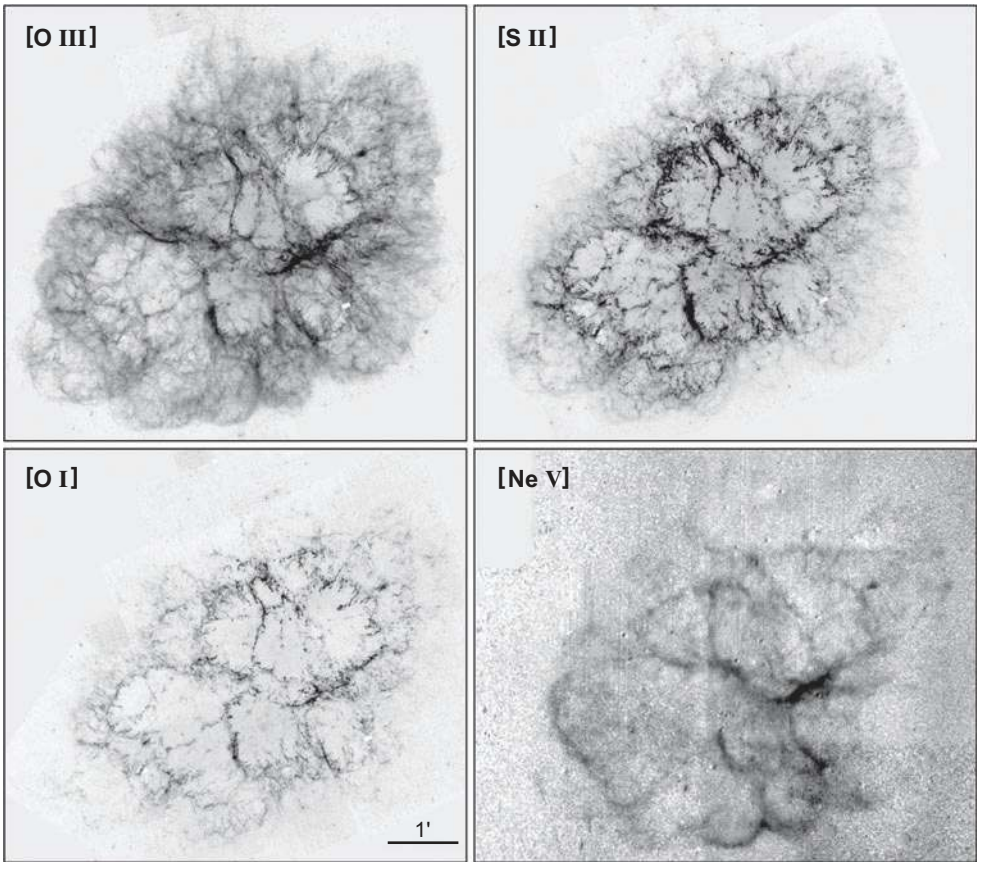

Figure 4

Emission line images of the Crab Nebula. The [O III], [S II], and [O I] images are mosaics of eight pointings taken with the HST WFPC2. The [Ne V] image is a much lower-resolution ground-based image (Loll et al. 2007). The classical filaments break up into complexes of knots and fingers, due largely to the action of Rayleigh-Taylor instabilities. Note that lower ionization emission is largely restricted to the cores of dense, self-shielding filaments, whereas emission from [O III] is much more uniformly distributed through the thick scalloped shell. The [Ne V] image shows the presence of a high-ionization skin that surrounds much of the nebula. This emission cannot be explained by photoionization and is interpreted instead as postshock emission behind the shock driven into surrounding freely expanding ejecta.

Initially, densities of order 10^{-2} cm^{-3} are quite common for interstellar cavities, especially for an environment that is known to have contained massive stars. In McKee & Ostriker's (1977) classic model of the ISM, the most common phase of the ISM has a density $n \sim 0.003$ cm^{-3}. The Local Bubble in which the Sun sits, which is thought to have formed as a result of star formation over the last 25–60 Myrs, is more than 100 pc across (comparable to the ~130 pc bubble surrounding the Crab) and has a density of ~0.01 cm^{-3} (Frisch 2007). Bubbles such as these are easily large enough to hold the freely expanding thousand-year-old remnant of a typical Type II supernova. Similarly, the ejecta around the Crab, which is seen in absorption in C IV, is highly ionized by the synchrotron emission escaping from the Crab, and temperatures of ~20,000 K have been observed in the body of the nebula itself. Because the density of ejecta must fall off more steeply than r^{-2}, both the ionization parameter and the mean energy of ionizing photons should increase outward in the ejecta. Warm, ionized ejecta is therefore to be expected. In short, current efforts to

detect an outer ejecta-driven shock around the Crab fail to rule out the existence of such a shock. Nor do they require an underluminous supernova.

In summary, after a long search, studies of the shock at the edge of the synchrotron nebula and direct spectroscopic evidence of C IV absorption provide strong evidence that a freely expanding supernova remnant surrounds the visible Crab Nebula, as originally hypothesized by Chevalier (1977). The Crab Nebula that we see is a pulsar-powered bubble within this larger, freely expanding remnant. Further, though we still do not know the energy of SN1054, there appears to be little real evidence that it was underluminous. Putting current searches for the outer shock in the Crab into appropriate context, had a typical Type II SN occurred within the Sun's Local Bubble 1000 years ago, the brightness of the outer shock would fall below current detection limits. The best analog for the Crab is probably SNR 0540–69.3 in the LMC, which has an inner object that is Crab-like in almost all regards, but around which an X-ray shell containing ~30–40 $M_\odot$ is seen (Seward & Harnden 1994, Hwang et al. 2001).

Until further observations provide better direct constraints, the simplest working assumption is perhaps that SN1054 was a typical Type II supernova that occurred within a large, low-density cavity and that the majority of the mass and the kinetic energy of the ejecta reside outside the visible Crab.

4. THE INTERNAL STRUCTURE OF CRAB FILAMENTS IS COMPLEX

Above I discuss the morphology of the thermal filaments in the Crab. I now turn attention to their internal structure.

4.1. There Is Dust in the Crab Nebula

The presence of dust in the Crab Nebula was originally inferred from the presence of a peak in the infrared spectrum around 50 μm (Glaccum et al. 1982, Marsden et al. 1984). Based on the infrared luminosity of the dust, Mezger et al. (1986) estimated a total grain mass of ~0.03 $M_\odot$, implying an overall dust-to-gas ratio of about 1:200, comparable to or somewhat lower than interstellar values. Marsden et al. (1984) estimate a dust mass in the range of 0.005–0.03 $M_\odot$. In their more detailed analysis based on *Spitzer* observations of the Crab, Temim et al. (2006) estimate dust masses ranging from ~0.001–0.015 $M_\odot$, depending on assumptions about dust size, composition, and temperature. Assuming a gas mass of 2–5 $M_\odot$ (Fesen, Shull & Hurford 1997), this implies an overall dust-to-gas ratio in the range of 0.0002–0.015, with lower values preferred. Although this range is broad, these values are typically lower than the interstellar ratio of ~0.01.

Dust is also seen in the Crab in extinction against the background of the synchrotron nebula. The first detections of dust extinction were those of Fesen & Blair (1990) and Hester et al. (1990). As noted above, HST observations show that the dust absorption features are even more strongly concentrated in the cores of filaments than is emission from [O I] (Hester et al. 1996, Blair et al. 1997), showing that much of the dust in the Crab is found in dense gas. Loll et al. (2007) find that all low-ionization filament cores on the front side of the Crab probably contain dust. Assuming typical values for the ratio of dust mass to extinction, Sankrit et al. (1998) find that the dust-to-gas ratio in one prominent Crab filament may be as high as ~0.1, a factor of 10 higher than typical of the ISM. Loll et al. (2007) find that a value of 0.03 may be more representative. Like the overall estimates of dust mass, estimates of the dust-to-gas ratio are quite uncertain, depending as they do on assumptions about grain properties and the amount of undetected neutral and molecular gas present in the cores of filaments. Even so, taken at face value the dust in the Crab may be

more strongly concentrated in filament cores than is the gas. It is also possible that the dust in the Crab, which has condensed from supernova ejecta, has significantly different optical properties than typical ISM dust.

4.2. Crab Filaments Have Stratified Ionization Structures

Most of the emission from the filaments can be understood as photoionization by the hard continuum from the synchrotron nebula (Henry & MacAlpine 1982, Pequignot & Dennefeld 1983). In these 1D models, slabs of gas are photoionized by the synchrotron continuum. The density and thickness of the slabs are then varied to match observed line strengths. These models demonstrate that power-law photoionization can account for many aspects of the spectra of Crab filaments. Even so, subsequent high-resolution images of the Crab in the light of different emission lines (**Figure 4**) reveal morphological and ionization structures that are far more complex than those assumed in the early models.

High-resolution observations of the Crab Nebula obtained with HST show that the morphology of thermal filaments in the Crab differs markedly between different emission lines. Emission from low-ionization lines is strongly localized in concentrated knots, whereas emission from high-ionization species is more diffuse. Sankrit et al. (1998), for example, found that 80% of [O I] emission in the Crab arises from structures smaller than 0.5 arcsec, whereas only 10% of [O III] emission arises in such compact structures. Close examination of the structure of filaments shows a range from typically small structures in which all lines originate from the same volume, to larger structures that show a strongly stratified ionization structure. **Figure 5** shows one such finger. The [O III] image of this finger shows a hollow envelope surrounding a core of emission seen in

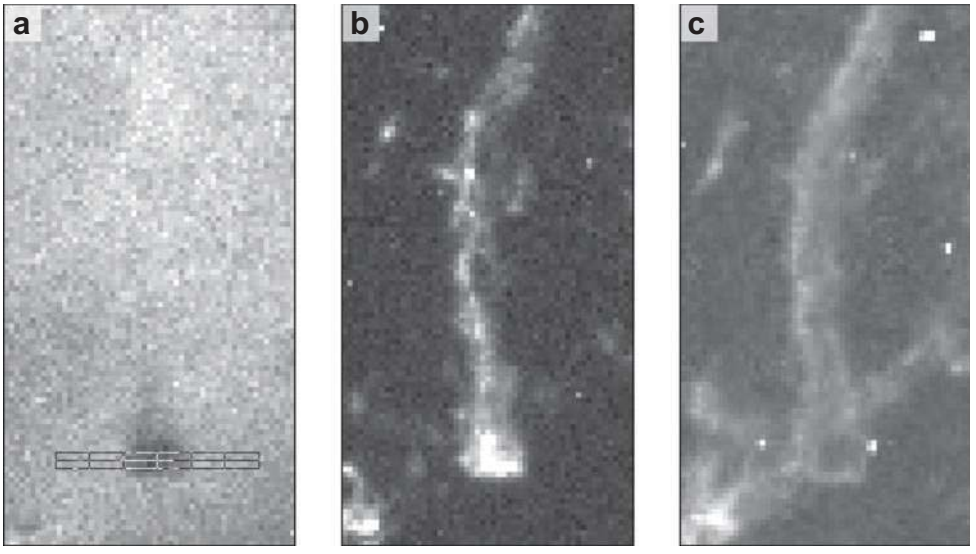

Figure 5

A prominent Rayleigh-Taylor finger seen in (*a*) continuum emission, (*b*) [O I] emission, and (*c*) [O III] emission (Sankrit et al. 1998). Note the stratified ionization structure. The self-shielded cores of prominent filaments show emission from low-ionization lines such as [O I] and even emission from H_2, and contain significant amounts of dust, seen here in extinction against the synchrotron background. The higher ionization [O III] emission is seen only on an extended envelope around the core of the finger.

[S II] and [O I]. Dust extinction is seen against the background of the synchrotron nebula as well, spatially coincident with the brightest [O I] emission. Graham, Wright & Longmore (1990) report the presence of H_2 in the spectra of two filaments as well. The picture of prominent filaments that emerges from this work is of dense structures with self-shielded cores that are externally ionized by continuum from the synchrotron nebula. This stratification is also apparent in differences in electron temperatures inferred using different nebular diagnostics in which, for example, [O III] temperatures are typically observed to be ~12,000–20,000 K, whereas [N II] temperatures are typically less than 10,000 K.

Sankrit et al. (1998) present photoionization models of cylindrically symmetrical structures representing R-T fingers, parameterizing radial density profiles using a core/envelope structure. These models quantitatively reproduce the observed surface brightness, ionization stratification, and electron temperatures for a variety of filaments. The column depths needed to reproduce the [O I], [S II], and [O III] profiles of prominent filaments are of order 10^{19} cm. This agrees with the column density that Graham, Wright & Longmore (1990) find necessary to shield H_2 from photodissociation over the age of the nebula. Although Sankrit et al. (1998) do not include molecular hydrogen in their models, they find that central densities of 1000–2000 cm^{-3} are required to match observed profiles and allow for higher densities in optically thick cores. Graham, Wright & Longmore (1990) find similar densities are required [$n(H_2) > 400$ cm^{-3}] if fast electrons are responsible for heating the H_2 in filaments. Graham, Wright & Longmore argue that the H_2 in the Crab filaments formed early in the expansion of the remnant, when densities were high, and has been shielded in the cores of filaments since then. Models of the development of R-T instabilities (e.g., Jun 1998) suggest that the more prominent fingers in the Crab formed within 100 to 200 years after the explosion.

4.3. Spectroscopic Studies of the Crab Show Abundance Variations

There have been numerous spectroscopic studies of the nebular abundances in the Crab (e.g., Miller 1978; Fesen & Kirshner 1982; Henry, MacAlpine & Kirshner 1984), most of which indicate that helium abundances in the bright filaments are higher than solar and vary significantly within the nebula. Uomoto & MacAlpine (1987) find that portions of the Crab have helium abundances that are close to solar, but in a band running from E to W across the object, helium may account for up to 90% of the mass. Abundance anomalies in massive elements have also been reported in all of these studies. Especially strong [Ni II] λ7378, in particular, may imply nickel abundances of 5 to 50 times the solar value, and nickel-to-iron abundance ratios as much as 60 to 75 times the solar value (MacAlpine et al. 1989). MacAlpine et al. (2007) interpret correlations between inferred abundances of various elements across the face of the nebula as evidence for gas produced by different stages of nuclear processing in the progenitor. These stages include material produced by the carbon-nitrogen-oxygen (CNO) cycle, products of helium burning and nitrogen depletion, and regions enriched by oxygen burning.

It is important to note that the complexity and variability of the stratified ionization structure of filaments in the Crab complicates interpretation of filament spectra, including measurement of nebular abundances. Similar effects have been seen in modeling of other photoionized environments such as H II regions, where changing conditions across sharply stratified ionization structure can lead to significant errors in abundances inferred using traditional methods (e.g., Sankrit & Hester 2000; Moore, Hester, & Dufour 2004). As noted above, the appearance of the Crab in the light of low- and high-ionization lines is radically different, down to subarcsecond scales (Sankrit et al. 1998, Blair et al. 1997, Loll et al. 2007). The ionization structure of the filaments in the Crab is extremely complex, and even very similar ions can occupy zones with

significantly different spatial extent and physical properties. For example, the ratio He I λ5876/Hβ is often taken as a straightforward indicator of helium abundance (Uomoto & MacAlpine 1987). However, photoionization models of cylindrical filaments show that, owing to photoionization of He I to He II in envelopes and enhancement of He I in cores, this ratio can be a factor of five lower in filament envelopes than in filament cores (Sankrit et al. 1998). Similar effects are seen in planetary nebulae (e.g., Kwitter & Henry 2001).

MacAlpine et al. (2007) argue against this being a major problem on the basis of line ratio correlations within the nebula, and it seems unlikely that features such as the high helium band can be explained away as being caused by ionization stratification effects. MacAlpine et al. (2007) do find that the localization of C I emission to shielded filament cores is likely responsible for the especially strong [C I] λ9850 emission in the Crab. As noted above, significant amounts of gas may reside in the neutral and molecular cores of filaments. For this reason special care must be taken in interpreting emission from any ionic species (e.g., [Fe II], [Ni II], [S II],[C I], [O I]) with an ionization potential less than that of hydrogen. Similar effects complicate abundances inferred from high-ionization species found in extended low-density envelopes. This is a likely explanation for the "argoknots" discussed by MacAlpine et al. (1994), selected on the basis of their strong [O III] and [Ar III] emission. Subsequent study using HST images (Schaller & Fesen 2002) showed that these knots are typical both in their morphology and their proper motion. The high [O III] and [Ar III] emission is a consequence of the fact that these knots have extended, high-ionization envelopes. Interpretation of spectra of the Crab could be improved by use of photoionization models similar to those of Sankrit et al. (1998), which have been fit to ionization profiles measured from HST images.

5. THE THREE-DIMENSIONAL STRUCTURE OF THE CRAB

Having discussed the small-scale structures in the ejecta, I turn attention to the large-scale 3D structure of the Crab.

5.1. Thermal Emission Forms a Thick Shell

Radial velocity studies show that thermal emission from the Crab Nebula is concentrated in a shell with a thickness of about 0.3–0.7 pc (Clark et al. 1983, Lawrence et al. 1995). As is apparent from **Figure 4**, the shell is far more uniform in emission from [O III] than it is in emission from lower ionization lines. Generally speaking, the brightness of the shell decreases toward the outer edge, while the ionization state increases. The brightest and lowest ionization emission is concentrated in what is referred to as the classical filaments, which are long known from ground-based observations. These bright features are found in the inner region of the shell, often forming an inner edge with fingers protruding inward farther still. HST observations of the Crab (Loll et al. 2007) show that R-T fingers can be seen throughout the shell, but the most prominent R-T fingers extend inward from the bright classical filaments. The drop-off in brightness of the visible synchrotron nebula corresponds roughly to the inner edge of this shell, while the radio synchrotron nebula is bounded by the high-ionization skin that defines the outer edge of the shell around all but the NW portion of the nebula.

Shell is actually something of a misnomer for the thick zone containing thermal emission. This region is perhaps better described in terms of a surface that has a bubbled morphology and is especially noticeable in the southeastern portion of the Crab. This surface has an appearance similar to that of the surface of a cumulus cloud. The scalloping of this structure around the boundary of the Crab has a wavelength of $\theta \sim \pi/10$. This is about the scale at which the Thin-Shell instability

comes to dominate the R-T instabilities responsible for smaller scale structures (Bucciantini et al. 2004). The Thin-Shell instability is a plausible origin for this large-scale bubble structure in the boundary of the Crab. In this description the brightest of the classical filaments are typically seen in the valleys between bubbles and may be regions of especially dense gas concentrated there by the Thin-Shell instability.

5.2. The Crab Nebula Is Symmetrical about the Pulsar Spin Axis

One of the most straightforward but fundamental results of recent observations of the Crab is that the 3D structure of the nebula is roughly symmetrical about an axis that runs from SE to NW through the nebula [position angle (PA) $\sim 130°$–$140°$ E of N], and tilts into the plane of the sky at its NW end by about 30°. This symmetry is perhaps most obvious in X-ray observations of the Crab synchrotron nebula obtained with *Chandra* (Weisskopf 2000), which show a pronounced torus with bipolar jets extending to the SE and NW of the pulsar. From the aspect ratio of the X-ray torus we infer that this axis is tipped into the plane of the sky by about 30°. The sense in which the torus is tipped into the sky is determined from Doppler brightening of the flow. The NW portion of this torus is brighter than the SE portion as a result of Doppler beaming of the flow. The same explanation applies to the brightness of the SE jet, in which emission is beamed toward us, as compared with the NW counterjet. The most careful fitting to the structure of the Crab torus is that of Ng & Romani (2004), who match the Crab torus with PA $= 126°.31 \pm 0.03$, an axis tilted into the plane of the sky by PA $= 26.97° \pm 0.03$, and a flow velocity through the torus of $0.550c \pm .001c$. This torus and associated structures can be seen in observations at visible and radio (Bietenholz, Frail & Hester 2001) wavelengths, bisects the well-known synchrotron wisps (Scargle 1969), and can be traced down to a bright knot of visible synchrotron emission seen at $\sim$0.5 arcsec to the SE of the pulsar (Hester et al. 1995). This axis of symmetry is roughly (but not exactly) aligned with the proper motion direction of the Crab pulsar (Ng & Romani 2006).

On the smallest scales at visible wavelengths, HST observations of the Crab synchrotron nebula (Hester et al. 1995, 2002) show the presence of a bright knot of synchrotron emission located only about 0.5 arcsec (1.5×10^{16} cm) to the SE of the pulsar, with no counterpart on the NW side. The feature is somewhat variable in both its position and its brightness and is highly polarized with the inferred nebular magnetic field aligned perpendicular to the symmetry axis of the nebula. There have been various suggestions for the physical nature of the knot, ranging from a quasi-stationary shock in the jet flow (Lou 1998), to Doppler beaming in the high-latitude wind (Del Zanna et al. 2006). Further along this axis is an irregular region of diffuse emission referred to as the Anvil, which marks the base of the X-ray and optical jet. The Anvil and a much fainter region of diffuse emission to the NW of the pulsar may be associated with shocks in the polar jet and counterjet, respectively. Wisp 2 is seen to be a portion of the front side of the equatorial torus and is actually composed of a complex of much sharper wisps with characteristic lateral scales of only about 0.2 arcsec ($\sim 5 \times 10^{15}$ cm). These fine wisps wrap around the front face of the torus. The Counter Wisp is associated within the back side of the torus. Wisp 1 is more complex. Hester et al. (1995) argue that Wisp 1 is the result of a line-of-sight superposition of features on the front side of the torus and a high-latitude halo, which includes the thin wisp on the back side.

The structure of the inner synchrotron nebula is imposed by the structure of the pulsar wind itself, and so the axisymmetry that we see is almost certainly associated with the spin axis of the pulsar. Arons (2008) reviews the physics of pulsars and pulsar winds. Recent models (e.g., Spitkovsky 2006) are beginning to clarify the nature of that wind, including the concentration of flow into the equatorial plane. The first images of the Crab taken with the *Chandra X-ray Observatory* showed that in addition to the larger X-ray torus, there is a bright and very sharp

inner ring. Weisskopf et al. (2000) identified this ring with location of the wind shock, suggesting that the energy flux from the pulsar wind is very sharply concentrated in the two jets and the equatorial wind.

The SE-NW symmetry axis of the Crab is also apparent on the largest scales in the nebula. Projected onto the plane of the sky, the nebula overall has a roughly elliptical shape ~2.9 pc × 4.0 pc in size with a major axis aligned with the spin axis of the pulsar. Lawrence et al. (1995) find that [O III] emission is especially faint in the SE and NW part of the Crab and that these regions line up best about an axis with PA ~ 125° E of N and inclined ~25° into the plane of the sky. Loll et al. (2007) found that the outer edge of the radio synchrotron nebula is reasonably well fit by a prolate spheroid with PA ~ 140° E of N, inclined ~30° into the plane of the sky. All of these are in close agreement with the axis inferred from the inner X-ray torus. Below I argue that the wind from the supernova precursor was probably organized about a N-S axis, in which case the overall spheroidal shape of the nebula is a consequence of the symmetry of the pulsar wind.

5.3. The Magnetic Structure Within the Crab Is Complex

Polarization provides the best available tool for studying the magnetic field structure within the Crab. The polarization of the Crab Nebula has been studied at wavelengths from radio through X-rays. Wilson (1974) was among the first to look at variations in polarization as a function of wavelength. Based on 6-cm radio depolarization by thermal filaments, he inferred that at least some filaments had line-of-sight magnetic fields of ~200 μG. The polarization in the inner nebula is strong and fairly uniform with an electric vector at PA ~ 155° (e.g., Schmidt, Angel & Beaver 1979). Because synchrotron radiation is polarized perpendicular to the magnetic field, this suggests that the field in the nebula is aligned from ENE to WSW (PA ~ 65°). When viewed in polarized light the Crab takes on an hourglass appearance with a N-S axis running through the position of the pulsar (Michel et al. 1991), again with the reconstructed magnetic field in the hourglass running roughly from E to W. Polarization observations show that the bays in the synchrotron nebula to the E and W of the pulsar, as well as other similar indentations, are the result of the magnetic field in the nebula wrapping around this torus (Michel et al. 1991; Fesen, Margin & Shull 1992).

The morphology of the interior of the Crab is quite different when viewed in polarized and unpolarized light (**Figure 6**). At HST resolution, fibrous structure dominates the polarized intensity (Hester 2007). The wisps in the equatorial torus are seen as sharp and prominent in polarized light, but even the parts of the nebula outside of the torus appear fibrous in polarized light. The brightest polarized light comes from the very front and the very back of the high-latitude halo to the NW of the pulsar, and from the knot located 0.5 arcsec SE of the pulsar. In contrast, the unpolarized intensity is dominated by much more diffuse and irregular emission. This includes clumps of emission that lie along along a high-latitude halo (Hester et al. 1995) and includes knots of emission seen at the base of the jet and the material along the length of the jet itself.

Although the overall polarization of the Crab might suggest a prominent N-S symmetry axis to the synchrotron nebula, interpretation of polarization observations of the Crab is complicated by the fact that the emission we see represents a line-of-light integral through the entire nebula, and hence tells us little about physically discrete features. When individual features are isolated from the background, magnetic fields reconstructed from polarization invariably align along the length of wisps and other fibrous textures in the nebula, with polarizations near 70% in some cases (**Figure 6*d***; Hester 2007). These observations show that wisps are flux tubes and show that the magnetic structure of the inner portion of the nebula follows the same axisymmetry discussed

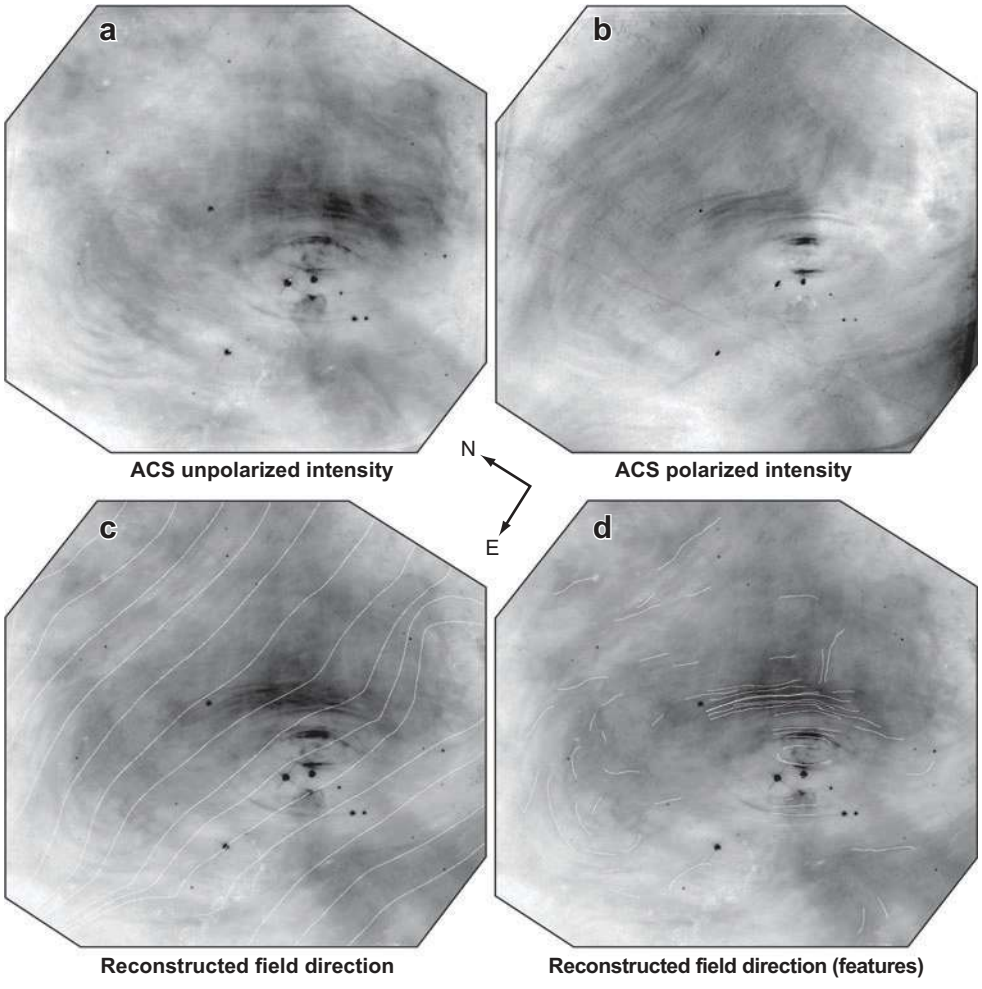

Figure 6

Hubble Space Telescope ACS observations of the polarization in the inner Crab Nebula. Note the differences in the appearance of the (*a*) unpolarized intensity and the (*b*) polarized intensity. The unpolarized intensity is much more diffuse, whereas the polarized intensity is dominated by wispy structures. The magnetic field direction inferred from the polarization observations (*c*) typically runs E-W across the body of the nebula, but when isolated from the background (*d*) magnetic fields invariably follow wisps and other striated structures, showing that striations in the nebula are magnetic flux tubes.

above. More generally, these observations allow fibrous structure throughout the synchrotron nebula to be interpreted as showing the local direction of the magnetic field.

Moving from the inner region into the body of the synchrotron nebula, high-resolution imaging of the synchrotron nebula in visible light (van den Bergh & Pritchet 1989, Hester et al. 1995) shows that fibrous structure with characteristic thickness of ~1–2 arcsec ($\sim 5 \times 10^{16}$ cm) runs throughout the nebula. These features loop around dense filaments, wrap around the X-ray torus, wrap around the X-ray jet and counterjet, and lie parallel to the boundary of the synchrotron nebula near its edge. Features in the outer nebula do not move outward like waves through the synchrotron nebula, but instead expand homologously with the outer edge of the synchrotron nebula (Hester et al. 1995). Some of these features are brighter in polarized light, whereas others are brighter in unpolarized light (Hester 2007), indicating that they represent layers of uniform magnetic field direction lying adjacent to (but unable to interpenetrate) layers of differing field direction. The field structure within the body of the Crab synchrotron nebula might be best described as taffy-like layers laid over and across each other at all angles. Within each layer the magnetic field is uniform, but there is no relationship between the alignment of the field between one layer and the next.

The spectral index structure in the Crab has been studied at all wavelengths from radio to X-rays, and there are discussions of various electron populations in the literature, generally distinguished by the wavelength regime in which they are observed. The overall result of these studies is apparent in **Figure 3**. The spectrum of the Crab is harder in the inner portions and softens toward the edge, consistent with synchrotron burn off. The details, however, are more complex. The X-ray torus has a photon index of ~1.9 (X-ray spectral index ~0.9; Mori et al. 2004), which drops to as low as ~4.4 (X-ray spectral index ~3.4) in the faint outer regions of the nebula (Seward, Tucker & Fesen 2006). The X-ray jet has a relatively harder spectrum core (photon index ~2.0) surrounded by a lower index sheath (photon index ~2.5; Mori et al. 2004). Especially deep X-ray images of the Crab (Hester et al. 1995; Seward, Tucker & Fesen 2006) show faint X-ray emission extending to near the outer boundary of the nebula. This X-ray emission is not uniform, but instead is seen in arcs and loops.

It is generally the case that the spectral index changes slowly along elongated fibrous structures, but can change abruptly across such structures. That is to say that spectral index changes slowly along field lines, but can change abruptly across field lines. This is easily understood because energetic particles are able to move easily along but not across field lines. Spectral index variations in the outer nebula might then be interpreted as due to changes in the length of the magnetically defined path that particles must traverse to reach a given point in the nebula. The most obvious examples of this sort of structure are extremely sharp edges in X-ray brightness that do not correspond to similar edges in visible light (Hester et al. 1995; Weisskopf et al. 2000). The field on one side of such an edge is presumably closely connected to the inner X-ray nebula, allowing X-ray emitting particles to survive the journey. Conversely, no similar short path exists from the inner nebula to the adjacent magnetic layer, which is correspondingly faint at X-ray wavelengths.

5.4. There Is a Pronounced Southeast-Northwest Asymmetry in the Crab

Although the Crab shows axisymmetry about the spin axis of the pulsar, there are pronounced differences in the properties of the SE and NW ends of that axis. The shock at the boundary of the Crab is radiative (shows a skin of [O III] and [Ne V] emission) and bounds the radio synchrotron nebula around most of the periphery of the nebula. The exception to this is in the NW portion of the remnant where the skin is not seen (Sankrit & Hester 1997). This is also the only region in the nebula where the synchrotron nebula extends beyond the edge of the visible filaments (Velusamy 1984). Sankrit & Hester (1997) explain this in terms of variations in the density of the ejecta into which the nebula is expanding. Assuming that the pressure within the synchrotron nebula is uniform, the shock velocity driven into the surrounding ejecta scales as $v_s \propto n^{-1/2}$. The cooling time behind the shock increases as ejecta density decreases. Sankrit & Hester (1997) found that for shock velocities around 195 km s^{-1} there is an abrupt transition. Below this velocity the cooling time is significantly less than the age of the Crab, allowing the visible skin to form and reach sufficient density at the interface to drive filament growth through R-T instabilities. Above this velocity, however, the postshock cooling time is longer than the age of the Crab. No visible skin appears, and absent dense cooled gas at the surface of the synchrotron nebula, filament growth stops. When this velocity is reached the synchrotron nebula is still bounded by the now nonradiative shock, but appears to break through the thermal filaments, as is seen on the NW end of the Crab. In addition to the absence of the skin, there are other indications that the shock velocity is higher in the NW part, including radial velocity measurements that show that the highest redshifted and blueshifted emission is seen in this part of the nebula (Lawrence et al. 1995).

High spatial resolution images of the filaments themselves also show a SE-NW asymmetry (Loll et al. 2007). There are fewer R-T fingers in the NW than in the SE, but the fingers are much longer, more prominent, and have a longer wavelength in the NW. The longer, better developed R-T fingers in the NW must have begun to form some time ago (e.g., Jun 1998), while the shorter fingers seen in the SE are more recent features, pointing to differences in the history of finger development at the two ends of the nebula. Because the most unstable wavelength for magnetic R-T instabilities is inversely proportional to the density jump across the interface, the short wavelengths in the SE might suggest that the postshock gas there is denser. The skin bridging between R-T fingers in the SE shows more low-ionization emission than does the skin in the NW, which is consistent with this interpretation.

Overall the properties of the skin, the observed filament velocities, and the morphology of R-T fingers together suggest that the preshock ejecta density is higher in the SE than in the NW. A likely explanation for this asymmetry involves the proper motion of the Crab pulsar. There have been numerous studies of the proper motion of the Crab pulsar (e.g., Wyckoff & Murray 1977, Caraveo & Mignani 1999). The most recent study, based on archival HST data taken over seven years, is that of Ng & Romani (2006), who obtain a best-fit proper motion of 14.9 ± 0.8 mas year^{-1} at a position angle of $278° \pm 3°$ E of N. This is misaligned by $26° \pm 3°$ from the axis that Ng & Romani (2004) fit to the pulsar wind torus. Kaplan et al. (2008) make the point, however, that uncertainties in reference frames and progenitor properties make it extremely difficult to establish either alignment or misalignment for individual sources. The observed proper motion corresponds to a velocity on the plane of the sky of around 140 km s^{-1}. If the proper motion is tilted into the plane of the sky by 30°, the space velocity of the pulsar would be about 160 km s^{-1}.

The space velocity of pulsars has a mean value of ~300–500 km sec^{-1} (e.g., Faucher-Giguère & Kaspi 2006). There is a significant literature on the possible origin of pulsar kicks; the most natural mechanism is some form of asymmetry in the supernova (e.g., Kalogera, Valsecchi & Willems 2008). The space velocity of the Crab pulsar is of fundamental importance in the interaction of the pulsar wind with freely expanding ejecta. The pulsar kick occurs at the time of the explosion, which means that the pulsar is moving with ejecta that was expelled at ~150 km s^{-1}. In the frame of reference of the pulsar the nebula expands freely, but is significantly lopsided. From the time of the explosion the pulsar wind has evolved through significantly more and denser material to the SE than it has to the NW. **Figure 7** shows an overview of the physical structure of the Crab Nebula described above.

5.5. There is a Secondary North-South Axis in the Crab

There is a second axis about which structure in the Crab Nebula is arranged. Uomoto & MacAlpine (1987) found that the He I λ5876/Hα ratio is especially high in a band running E-W across the nebula. Imaging Fabry-Perot studies (Lawrence et al. 1995) found that this feature extends circumferentially around the nebula and constitutes a significant pinch in N-S velocity ellipses (MacAlpine et al. 1989). Fesen, Margin & Shull (1992) note that the E and W synchrotron bays wrap around this feature and suggest that it might be a consequence of presupernova mass loss in the equatorial plane of the progenitor. Michel et al. (1991) find that the overall polarized intensity of the synchrotron nebula has an hourglass structure with a N-S axis (although see discussion of polarization, above). The stem on the northern edge of the nebula (van den Bergh 1970, Gull & Fesen 1982) is also roughly perpendicular to the plane of the E-W band. This cylindrical feature is seen in [O III] and [Ne V], encloses an extension in the radio synchrotron emission (Velusamy 1984), and in all other respects is a tube-like extension of the skin around the Crab (Sankrit & Hester 1997).

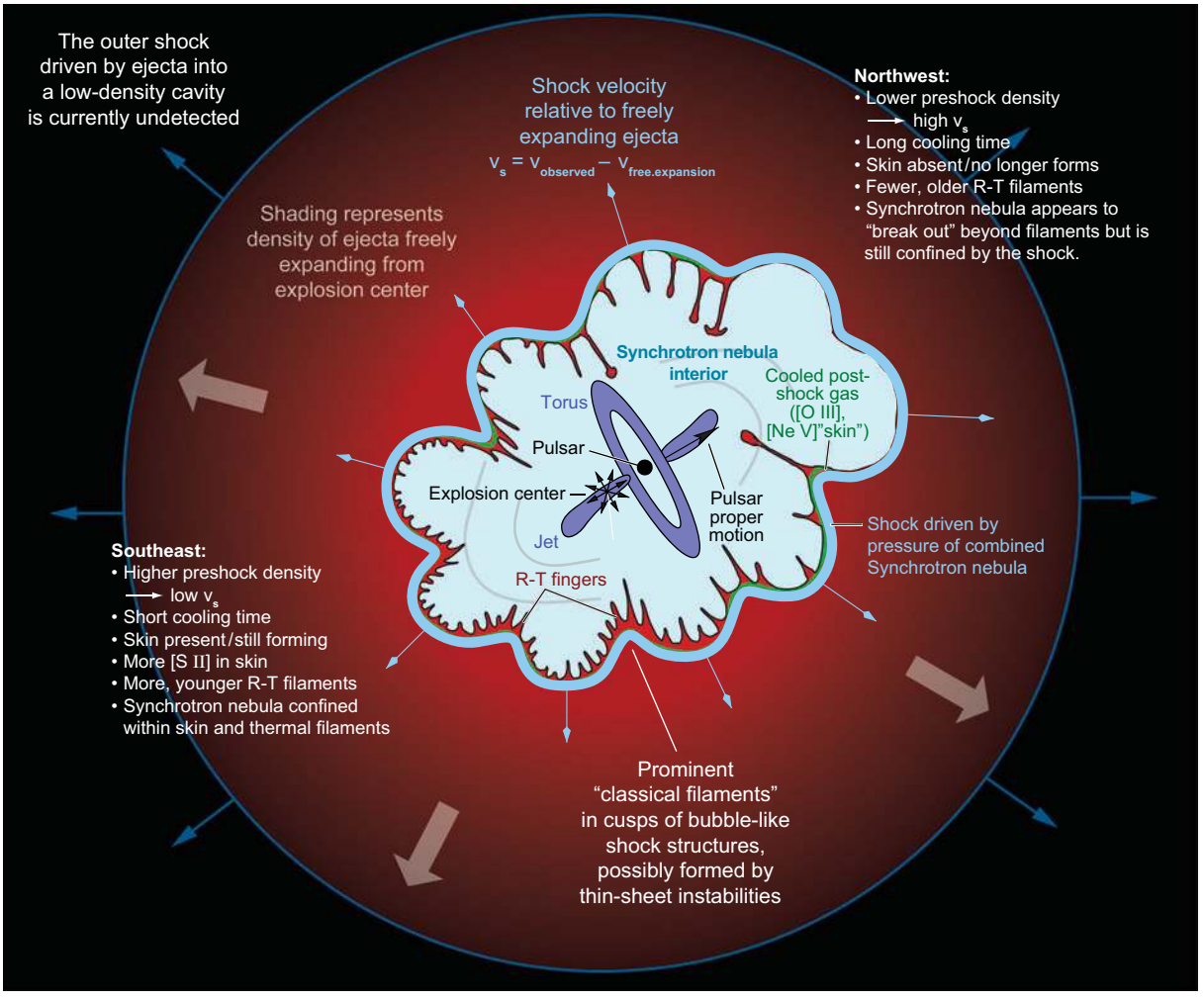

Figure 7

A summary of the structure of the Crab Nebula. The visible Crab consists of the synchrotron nebula, which is confined by thermal ejecta from the explosion. The pressure of the synchrotron nebula drives a shock into the surrounding freely expanding ejecta. This shock is radiative around most of the SE portion of the Crab and can be seen as a thin skin of [O III] and especially [Ne V] emission. The shock is nonradiative in the NW, where the synchrotron nebula extends beyond the boundary of the filaments. The SE-NW asymmetry can be understood as a consequence of the off-center location of the pulsar due to the velocity kick received by the pulsar at the time of the explosion. Rayleigh-Taylor (R-T) instabilities at the interface between the synchrotron nebula and the swept-up ejecta concentrate ejecta into small finger-like structures. The overall scalloped structure of the nebula may result from a thin-shell instability. The shock at the outer edge of the freely expanding ejecta has not been detected. (Features are not shown to scale.)

All core collapse supernovae that have been studied with techniques such as spectropolarimetry have proven to be strongly aspherical and frequently bipolar (e.g., Wheeler, Maund & Shizuka 2007; Wheeler & Wang 2008, in this volume), so such asymmetries are to be expected in the ejecta from SN1054. Further, the spin axes of neutron stars formed in these events need not be aligned with the symmetry axis of the explosion itself. Misalignment between the spin axis and kick velocity of the Crab pulsar provides direct evidence of such asymmetries. It is to be expected, therefore, that the pulsar wind powering the Crab expanded outward through a bipolar pattern

of ejecta. The features that suggest a N-S axis to the Crab (the high-He torus, velocity pinches, the stem, etc.) are associated with the distribution of ejecta, while the SE-NW asymmetry is seen in features imposed by the pulsar wind. The simplest hypothesis may be to associate the N-S axis with the explosion symmetry. The overall structure would then be the result of the pulsar wind, symmetrical about an SE-NW axis, pushing its way outward through the bipolar ejecta from the supernova. This might explain, for example, the S-shaped curve in the jet and counterjet.

6. DYNAMIC BEHAVIOR OF THE SYNCHROTRON NEBULA

The rapid variability of the Crab synchrotron nebula has been known for quite some time (Lampland 1921, Oort & Walraven 1956). The first detailed study of the dynamics of the Crab synchrotron nebula was that of Scargle (1969), who obtained images of the Crab every couple of months over a period of years. Although able to document variability in the inner nebula, Scargle was unable to distinguish between actual motion and oscillatory behavior. Based on data obtained with the ROSAT satellite, Greiveldinger & Aschenbach (1999) found evidence of X-ray variability in the torus, but again the nature of the variability was unclear. When higher-resolution images of the Crab were obtained with HST (Hester et al. 1995), it became clear that the timescale for variability could be much shorter than previously supposed. HST images show that fine structure in wisps is seen on scales of 10^{16} cm or less. At an assumed sound speed in the nebula of $c/\sqrt{3}$, appropriate for a particle-dominated relativistic plasma, the sound crossing time for such features is of order a few days.

Subsequent observations with HST and *Chandra* (Hester 1998, Hester et al. 2002, Mori et al. 2006) showed dramatic time evolution of features in the nebula. Hester et al. (2002) in particular conducted a temporal monitoring program in which simultaneous observations were taken with HST and *Chandra* over a period of ∼5 months (**Figure 8**). Prominent wisps in the equatorial torus of the Crab move outward with apparent speeds ranging from $\sim 0.35c$ to $\sim 0.5c$, which after correction for light travel-time effects can require space velocities as high as $\sim 0.7c$. The same features are seen in both the X-ray and visible light images. These velocities are far in excess of the velocities predicted in spherically symmetrical models (Kennel & Coroniti 1984a). Multidimensional models (e.g., Del Zanna et al. 2006) show that high velocities can arise as a result of expansion into lower pressure regions in a nonspherical flow.

There is strong asymmetry between wisps seen in the NW part of the torus and wisps seen in the SE. In comparison with wisps on the front (NW) side of the torus, features on the back (SE) side are fainter, have more open shapes, move more slowly (apparent velocities of $\sim 0.03c$ to $\sim 0.1c$), are longer lived, and are more bunched up. All of these differences can be accounted for by Doppler beaming and by light delay time effects in features moving toward and away from the observer at relativistic speeds. The single image fit of Ng & Romani (2004) to the Crab torus formally gives a velocity of $0.55c$ for material flowing through the torus, in good agreement with characteristic space velocities inferred from observed proper motions.

By combining the X-ray and optical movies of the Crab, Hester et al. (2002) put together the time evolution of a typical wisp in the equatorial region. Focusing attention on the near side of the torus, luminous material is first seen as it moves outward from the locus of the X-ray ring discussed by Weisskopf et al. (2000). The X-ray ring itself is composed of roughly two dozen knots that are highly variable but roughly stationary. This leaves little doubt that the X-ray ring is the shock in an especially intense portion of the pulsar wind that is confined very tightly to the equatorial plane of the pulsar. Polarization observations (Hester 2007) show that the optical counterparts of these knots are prominent in unpolarized light, indicating that they are regions of highly disordered magnetic fields.

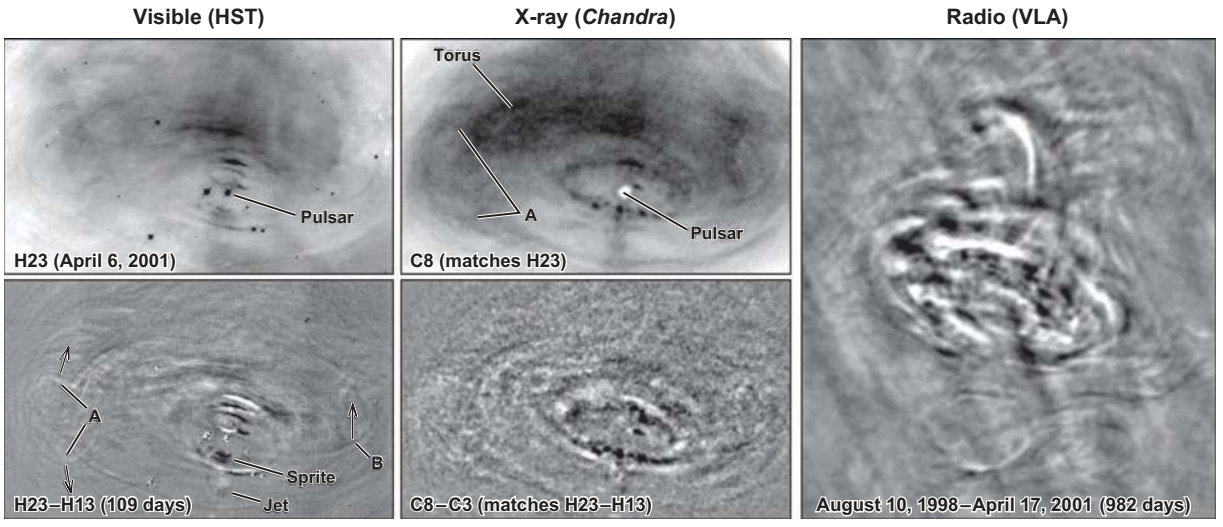

Figure 8

Illustrations of the dynamics of the inner Crab synchrotron nebula. The leftmost panels show *Hubble Space Telelscope* observations of changes in visible light over 109 days. The center panels show *Chandra* observations of changes in X-ray emission over the same period. The rightmost panel (not to scale) shows Very Large Array observations of changes in radio emission over 982 days.

The material leaving the ring is typically fairly diffuse and irregular, and is most luminous at X-ray wavelengths. Knots in the ring are seen to undergo outbursts from which puffs of outwardly moving material emerge. As the material moves outward from the inner ring into the region of the bright torus, it is compressed in the direction perpendicular to the flow, leading to the appearance of discrete, dynamic, and short-lived wisps. Typically a wisp appears as a diffuse feature with a width of order 1" moving at $\sim 0.5c$, then brightens and sharpens very quickly. Then over a period of a few months the wisp becomes fainter, spreads out, and blends into the background of the torus. Most but not all wisps appear to decelerate somewhat during this process, although some change speed very little, or may actually appear to accelerate somewhat. (These variations could be due to differences in direction of wisp motion as well as changes in space velocity.) There is, however, a general trend to see fast-moving features in the inner portion of the torus. Slower-moving and less sharply defined features toward the outer edge of the torus have typical velocities of $\sim 0.03c$. Observations taken over a 15-month baseline (Mori et al. 2006) show that especially bright wisps appear every 6 months or so, but these are the top end of a spectrum of wisps that appear more frequently.

Wisps from the torus are also seen at radio wavelengths (Bietenholz, Frail & Hester 2001), with a velocity of $0.24c$ reported for one feature. This velocity is slower than what is typical of bright optical and X-ray wisps, and subsequent observations (Bietenholz et al. 2004; **Figure 8**) show that radio wisps in the inner nebula do not always match up well with wisps seen in visible light. It is also the case that bright rapidly moving wisps stand out more in X-rays than in visible light and are confined to the volume of the bright X-ray torus, suggesting that these features have particularly hard particle energy spectra. Taken as a whole, the data seem to indicate that the particle energy spectrum in wisps evolves appreciably over their life cycle. The presence of wisps in the radio at all is surprising. Models of particle acceleration at the wind shock cannot account for the radio electrons in the Crab (e.g., Arons 1998, Atoyan 1999), and modelers frequently suggest that perhaps radio-emitting electrons are left over from an earlier phase in the evolution

of the pulsar or are injected in a different part of the pulsar wind. The existence of radio wisps strongly implies that radio electrons are being accelerated in the same equatorial region as the higher-energy electrons responsible for optical and X-ray emission.

Wisp motions do not always remain radial as they move outward through the torus. Movies of the Crab show the presence of wisps in the outer portions of the torus moving along with, rather than perpendicular to, the direction of the axis. There are partial loops seen in both the X-ray and optical images that wrap around the torus and expand outward about $0.03c$. As discussed above, polarization observations show that these loops trace the structure of the magnetic field. Although probably not entirely poloidal, these features violate all of the symmetry assumptions made to date in efforts to model the structure of the Crab. Plasmas with crossed magnetic fields cannot interpenetrate, so the magnetic field geometry indicates that the torus itself is being confined as it pushes out into the body of the nebula. Based on the field morphology, the torus is perhaps best described as a donut that is inflated from within by the equatorial wind and is confined externally by complex nonaxial fields. The clear break in field geometry, X-ray brightness, and X-ray spectral index at the edge of the torus shows that the common assumption of smooth expansion of an axial field into the larger nebula is incorrect.

In addition to the wisps, temporal monitoring observations also show that the jet to the SE of the pulsar is a dynamical feature along which material flows at speeds of $\sim 0.4c$. This flow slows along the length of the jet, which is seen to push outward into the body of the nebula at speeds of $\sim 0.03c$. Interestingly the jet is not seen at radio wavelengths (Bietenholz et al. 2004). The jet flows outward from the region of the sprite, which consists of a collection of bright and highly variable knots. These knots undergo outbursts from which material emerges and are prominent in unpolarized light, indicating the presence of disordered magnetic fields. Material moving outward from one outburst was center filled in X rays and had the structure of a bow shock in HST images. These knots look and behave in almost all respects like the knots seen in the X-ray ring and seem most likely to be the same type of unstable quasi-stationary shock in a polar jet.

7. MODELS OF THE SYNCHROTRON NEBULA HAVE BECOME MORE SOPHISTICATED

Models of PWN, and the Crab PWN in particular, have grown far more sophisticated since the pioneering work of Rees & Gunn (1974) and Kennel & Coroniti (1984a,b). One of the main improvements over previous work is multidimensional treatment of the wind. This work has been discussed in a number of recent reviews (e.g., Gaensler & Slane 2006, Arons 2008), and so will not be reviewed here in detail. The recent work of Del Zanna et al. (2006) represents the state of the art in such modeling and is of particular current note. These researchers present axisymmetric calculations of pulsar winds assuming toroidal magnetic fields and latitudinal variations in pulsar wind properties. Among other results they provide a compelling explanation for the extremely rapid speeds exhibited by the wisps, which are well in excess of the maximum of $c/\sqrt{3}$ in 1D models. These models also provide insight into the behavior of the flow at high latitudes and provide a plausible interpretation for the knot near the pulsar in terms of Doppler boosting.

This excellent work provides the opportunity for a cautionary note, however. At this point observations of the Crab are of exceedingly high quality and demand a very high standard when being compared with theory. Current models are axisymmetric, have latitudinal variations in wind properties, and allow for softening of the synchrotron spectrum with distance from the pulsar. Such models will necessarily produce toroidal structure that may be tuned to superficially resemble the Crab. That does not mean, however, that physical interpretations of structure in the Crab based on such models are correct. There are a number of important respects in which current models fail

to reproduce the observations. For example, observations show that the Crab synchrotron torus is confined by external magnetic fields that have a poloidal component (Hester et al. 2002, Hester 2007), violating the symmetry assumptions of any strictly toroidal model. The models predict that the jet in the Crab should be hollow and highly polarized. In fact, the jet is center filled with a harder spectrum core and softer spectrum sheath (Mori et al. 2004), and exhibits low polarization (Hester 2007). The models show nothing like the exceedingly dynamic and largely unpolarized knots seen in the sprite at the base of the jet.

The wisps in the Crab provide another cautionary example when applying theory to observations. Although current models do provide an explanation for high flow velocities, they do not predict the dynamic behavior of the wisps. There have been a number of theoretical ideas about the nature of the wisps (e.g., drift instabilities, Chedia et al. 1997; Kelvin-Helmholtz instabilities, Begelman 1999). Spitkovsky & Arons (2004) present an interesting model in which wisps result from an ion cyclotron instability in a wind whose energy flux is dominated by ions rather than electron-positron pairs (Gallant & Arons 1994). They make comparisons with HST observations of wisp motions, but acknowledge that these are qualitative and that there are problems with the model such as the apparent lack of Doppler brightening between the front and back sides of the *Chandra* ring. The model also remains a 1D attempt to describe features whose behavior is manifestly multidimensional.

Hester (1998) and Hester et al. (2002) propose that the wisps are the result of synchrotron cooling instabilities in a flow that is undergoing a transition from being particle dominated to being field dominated. They note that the wisps form, evolve, and dissipate within the X-ray torus, the region responsible for most of the bolometric luminosity of the Crab. The possible significance of radiative losses is a problem that applies not only to the wisps, but to models of the Crab more generally (Foy 2007). Current models (e.g., Del Zanna et al. 2006) include radiative losses while following the synchrotron emission from the plasma, but they do not couple those losses back into the dynamics of the flow itself. One argument typically made to support this approximation is that synchrotron losses are only about 10% of the pulsar's spin-down luminosity. First, this is an underestimate. As discussed above, 25% is a more representative number. Even in the best-fit model from Kennel & Coroniti (1984b), the synchrotron losses are about 40% of the pulsar's mechanical luminosity. Foy (2007) adds radiative losses to the Kennel & Coroniti model and shows that cooling can affect the dynamics in significant ways, though keeping losses within observational constraints. Second, synchrotron losses are concentrated in very sharp features. Spitkovsky & Arons (2004) argue that the X-ray spectrum is too flat for high-energy particles to carry the pressure (as must be the case for the instability to operate) and that particle lifetimes are too long.

These arguments that synchrotron losses are unimportant to the dynamics overlook the heterogeneous structure of the Crab synchrotron nebula. The spectrum of the synchrotron nebula shown in **Figure 2** represents the total spectrum of the Crab, rather than the spectrum at any given location. Most of the energy from the Crab is radiated in the optical through X-ray bands. From **Figure 2**, the integrated spectral energy density νL_ν is flat between the visible and soft X-ray portions of the spectrum, giving a spectral index $\alpha \sim 1 (L_\nu \propto \nu^{-\alpha})$ across this energy range. The inferred particle spectral index is then $p = 2\alpha + 1 \sim 3$ $[n(\gamma) \propto \gamma^{-p}]$—too steep for the more energetic particles to carry the energy. If the particle pressure is carried by the $\gamma \sim 5 \times 10^5$ particles responsible for optical emission, and assuming a magnetic field of 300 μG, this corresponds to particle lifetimes $\tau = \frac{E}{\dot{E}} = \frac{\gamma m_e c^2}{c_2 H^2 (\gamma m_e c^2)^2} \sim 300$ years. Using these values, we might infer that radiative energy losses are unimportant in the dynamics of the nebula. This is the objection from Spitkovsky & Arons (2004).

Figure 3, however, shows that the X-ray emission from the Crab comes from a much smaller volume than does the visible emission. Comparing the X-ray and visible light images combined to form **Figure 3**, we estimate that the ratio of the X-ray and optical volume emissivities in the X-ray torus is roughly a factor of 10 higher than the nebular average, corresponding to a spectral index $\alpha \sim 0.5$, and $p \sim 2$ for the torus. The spectrum of individual wisps is even harder. This difference is crucial because for $p < 2$, the particle pressure in the plasma is dominated by high energy particles with $\gamma \sim 2 \times 10^7$. Combining this with inferred minimum-energy magnetic fields within the bright wisps themselves of ~2000 μG (Hester et al. 1995) gives particle lifetimes of $\tau \sim 0.2$ years. Using these values, we might conclude that radiative losses could easily drive the dynamics of the wisps. Although it is unclear whether synchrotron cooling plays a key role in the evolution of the wisps, it is clear that calculations based on bulk properties of the nebula cannot meaningfully be used to rule out processes occurring on smaller scales and in specific features. The Crab presents a very heterogeneous environment, and model comparisons need to be done with care, making full use of available observational data.

8. AN EVOLVING PICTURE OF THE CRAB NEBULA

Over the past 15 years, a host of new observations have lead to fundamental changes in our physical understanding of the Crab Nebula. Rather than a free expansion supernova remnant that happens to contain a luminous pulsar, the visible Crab Nebula is more properly thought of as a pulsar wind nebula evolving within the much larger freely expanding remnant of SN1054. The pressure of the confined synchrotron nebula drives a shock into the surrounding ejecta and has swept up and compressed some fraction of this gas. Nonlinear development of hydromagnetic instabilities at the interface between the synchrotron nebula and the shocked ejecta have further structured the swept-up ejecta into dense complex filaments, which in turn are photoionized by UV and soft X-ray emission from the synchrotron nebula. It is these filaments, together with the exquisitely dynamic synchrotron nebula itself, that make up the visible nebula that we see today. The outer shock driven by the freely expanding remnant lies far beyond the visible edge of the Crab and remains undetected. The award for prescience regarding the Crab should go to Rogier Chevalier, who proposed much of this description three decades ago.

The Crab remains perhaps the single best object in the sky for studying a wide range of interlocking astrophysical problems, and a great deal of observational and theoretical work remains to be done. Beginning with the ejecta, the dense cores of the filaments are poorly understood. Infrared imaging of H_2 emission and observations of CO with ALMA will be important. ALMA will also image thermal emission from dust in the Crab filaments that, together with multiwavelength studies of dust absorption properties with HST WFC3, might be used to better constrain properties of dust condensed directly from the supernova ejecta. High-resolution imaging of filaments throughout the Crab can be used to constrain the physical structure of filaments, allowing more realistic 3D photoionization models to be constructed and used to better analyze ground-based spectroscopy. The history and evolution of the shock and instabilities in the contact discontinuity at the edge of the synchrotron nebula remain fertile and observationally well-constrained theoretical problems. Further studies of the extended remnant around the Crab are needed to finally understand the nature of the progenitor. Though continued searches for the outer shock are important, HST COS observations of C IV absorption in the spectrum of the pulsar and perhaps observations of resonant scattering of synchrotron emission in C IV by the ejecta hold promise as well.

The Crab synchrotron nebula remains the only place in the sky where relativistic astrophysical phenomena can be studied with the spatial and temporal resolution needed to constrain the relevant physics. The magnetic field in the wind shock appears tangled rather than toroidal, so the question

of particle acceleration is not simple. As a real theoretical problem, the 3D interior structure of the magnetic field in the synchrotron nebula is untouched. Confinement of the torus by poloidal fields and leakage of field out of the torus into the main body of the nebula are parts of this larger problem. Better studies of the effects of synchrotron cooling and the possibility of ions in the flow are also needed. Until these questions of basic physics are better understood even sophisticated axisymmetrical relativistic MHD calculations with torroidal fields remain toy models. Very long-term monitoring of the dynamics of the inner Crab, probably with ground-based adaptive optics, is needed to better constrain models of their evolution. Finally, observations of the synchrotron nebula provide strong but not well-understood boundary conditions on the pulsar wind itself.

These represent a small sample of the wealth of problems that remain to be tackled. The common theme in all of this work is the opportunity for very well-constrained and detailed (and therefore physically meaningful) comparisons between theory and observation. The high quality of available observations makes this a difficult game, however. Oversimplified models are no longer good enough. We have reached the point that work on the Crab needs to be done very carefully by making comprehensive use of available observational data, and meanwhile being rigorously honest about how approximations and assumptions are justified and how well theoretical predictions truly fare.

DISCLOSURE STATEMENT

The author is not aware of any biases that might be perceived as affecting the objectivity of this review.

ACKNOWLEDGMENTS

I would like to thank the many many people who have contributed to my own work on the Crab over the years. This ranges from the staff at STScI and CXC, who made difficult coordinated HST and *Chandra* observations possible, to countless colleagues who have contributed to the work. I would like to thank in particular my students who have worked on the Crab, including Ravi Sankrit, Joe Foy, Allison Loll, and Heidi van Tassell.

LITERATURE CITED

Alfvén H, Herlofson N. 1950. *Phys. Rev.* 78:616

Arons J. 1998. In *The Relationship Between Neutron Stars and Supernova Remnants*, ed. R Bandiera, E Masini, F Pacini, M Salvati, L Woltjer, Mem. Soc. Astron. Italiana, 69(4):989

Arons J. 2008. In *Springer Lecture Notes. "Neutron Stars and Pulsars, 40 years after the discovery,"* ed. W Becker, In press

Atoyan AM. 1999. *Astron. Astrophys.* 346:L49

Atoyan AM, Aharonian FA. 1996. *MNRAS* 278:525

Bandiera R, Pacini F, Salvati M. 1983. *Astron. Astrophys.* 126:7

Begelman MC. 1999. *Ap. J.* 512:755

Bejger M, Haensel P. 2003. *Astron. Astrophys.* 405:747

Bietenholz MF, Frail DA, Hester JJ. 2001. *Ap. J.* 560:254

Bietenholz MF, Hester JJ, Frail DA, Bartel N. 2004. *Ap. J.* 615:794

Bietenholz MF, Kassim N, Frail DA, Perley RA, Erickson WC, Hajian AR. 1997. *Ap. J.* 490:291

Bietenholz MF, Kronberg PP, Hogg DE, Wilson AS. 1991. *Ap. J.* 373:L59

Blair WP, Davidson K, Fesen RA, Uomoto A, MacAlpine GM, Henry RBC. 1997. *Ap. J. Suppl.* 109:473

Blair WP, Long KS, Vancura O, Bowers CW, Conger SD, et al. 1992. *Ap. J.* 399:611

Bucciantini N, Amato E, Bandiera R, Blondin JM, Del Zanna L. 2004. *Astron. Astrophys.* 423:253

Caraveo PA, Mignani RP. 1999. *Astron. Astrophys.* 344:367
Chandrasekhar S. 1961. *Hydrodynamic and Hydromagnetic Stability*. Oxford: Oxford Univ. Press
Chedia O, Lominadze J, Machabeli G, Mchedlishvili G, Shapakidze D. 1997. *Ap. J.* 479:313
Chevalier RA. 1977. In *Supernovae*, ed. DN Schramm, 66(53):202. Dordrecht: Reidel
Chevalier RA, Fransson C. 1992. *Ap. J.* 395:540
Chevalier RA, Gull TR. 1975. *Ap. J.* 200:399
Clark DH, Murdin P, Wood R, Gilmozzi R, Danziger J, Furr AW. 1983. *MNRAS* 204:415
Clark DH, Stephenson RR. 1977. *The Historical Supernovae*, Oxford: Pergamon
Cocke WJ, Disney MJ, Taylor DJ. 1969. *Nature* 221:525
Comella JM, Craft HD, Lovelace RVE, Sutton JM, Tyler GL. 1969. *Nature* 221:453
Davidson K. 1979. *Ap. J.* 228:179
Davidson K, Fesen RA. 1985. *Annu. Rev. Astron. Astrophys.* 23:119
Del Zanna L, Volpi D, Amato E, Bucciantini N. 2006. *Astron. Astrophys.* 453:621
Dombrovsky VA. 1954. *Dokl. Akad. Nauk SSSR* 94:1021
Duyvendak JJL. 1942. *Publ. Astron. Soc. Pac.* 54:91
Faucher-Giguère CA, Kaspi VM. 2006. *Ap. J.* 643:332
Fesen RA. 1997. *Astron. J.* 113:354
Fesen RA, Blair WP. 1990. *Ap. J.* 351:L45
Fesen RA, Kirshner RP. 1982. *Ap. J.* 258:1
Fesen RA, Margin CL, Shull JM. 1992. *Ap. J.* 399:599
Fesen RA, Shull JM, Hurford AP. 1997. *Astron. J.* 113:354
Foy JP. 2007. *The Role of Synchrotron Cooling in Modeling the Dynamic Wisps of the Crab Nebula*. PhD thesis. Ariz. State Univ., Tempe. 214 pp.
Frail DA, Kassim NE, Cornwell TJ, Goss WM. 1995. *Ap. J.* 454:L129
Frisch PC. 2007. *Space Sci. Rev.* 130:355
Gaensler B, Slane P. 2006. *Annu. Rev. Astron. Astrophys.* 44:17
Gallant YA, Arons J. 1994. *Ap. J.* 435:230
Glaccum W, Harder DA, Loewenstein RF, Pernic R, Low FJ. 1982. *Bull. Am. Astron. Soc.* 14:612
Graham JR, Wright GS, Longmore AJ. 1990. *Ap. J.* 352:172
Greiveldinger C, Aschenbach B. 1999. *Ap. J.* 510:305
Gull TR, Fesen RA. 1982. *Ap. J.* 260:L75
Henry RBC, MacAlpine GM. 1982. *Ap. J.* 258:11
Henry RBC, MacAlpine GM, Kirshner RP. 1984. *Ap. J.* 278:619
Hester JJ. 1998. In *Neutron Stars and Pulsars: Thirty Years after the Discovery*, ed. N Shibazaki, pp. 431-436. Tokyo: Univ. Acad. Press, 564 pp.
Hester JJ. 2007. HST ACS Polarization Observations of the Crab Nebula. *Bull. Am. Astron. Soc.* 211:100.26
Hester JJ, Graham JR, Beichman CA, Gautier TN III. 1990. *Ap. J.* 357:539
Hester JJ, Mori K, Burrows D, Gallagher JS, Graham JR, et al. 2002. *Ap. J.* 577:L49
Hester JJ, Scowen PA, Sankrit R, Burrow CJ, Gallagher JS III, et al. 1995. *Ap. J.* 448:240
Hester JJ, Stone JM, Scowen PA, Jun B-I, Gallagher JS III, et al. 1996. *Ap. J.* 456:225
Hwang U, Petry R, Holt SS, Szymkowiak AE. 2001. *Ap. J.* 560:742
Jun B-I. 1998. *Ap. J.* 499:282
Kalogera V, Valsecchi F, Willems B. 2008. In *40 Years of Pulsars: Millisecond Pulsars, Manetars, and More*, ed. C Bassa, Z Wang, A Cumming, VM Kaspi, 983:433–41. AIP Conf. Proc. New York: Springer-Verlag
Kaplan DL, Chatterjee S, Gaensler BM, Anderson J. 2008. *Ap. J.* 677:1201
Kennel CF, Coroniti FV. 1984a. *Ap. J.* 283:694
Kennel CF, Coroniti FV. 1984b. *Ap. J.* 283:710
Kwitter KB, Henry RBC. 2001. *Ap. J.* 562:804
Lampland CO. 1921. *Publ. Astron. Soc. Pac.* 33:79
Lawrence SS, MacAlpine GM, Uomoto A, Woodgate BE, Brown LW, et al. 1995. *Astron. J.* 109:2635
Loll A, Hester JJ, Sankrit R, Blair WP. 2007. A Northwest-Southeast Asymmetry in the Structure of the Crab Nebula. *Bull. Am. Astron. Soc.* 211:100.25
Lou Y-Q. 1998. *MNRAS* 294:443

Lundmark K. 1921. *Publ. Astron. Soc. Pac.* 33:225
Lyne AG, Pritchard RS, Smith FG. 1988. *MNRAS* 233:667
MacAlpine GM, Ecklund TC, Lester WR, Vanderveer SJ, Strolger L-G. 2007. *Ap. J.* 133:81
MacAlpine GM, Gordo M, Lawrence SS, Brown BA, Uomoto A, et al. 1994. *Ap. J.* 432:L131
MacAlpine GM, McGaugh SS, Mazzarella JM, Uomoto A. 1989. *Ap. J.* 342:364
Marsden PL, Gillett FC, Jennings RE, Emerson JP, de Jong T, Olnon FM. 1984. *Ap. J.* 278:L29
Mauche CW, Gorenstein P. 1989. *Ap. J.* 336:843
Mayall NU, Oort JH. 1942. *Publ. Astron. Soc. Pac.* 54:95
McKee CF, Ostriker JP. 1977. *Ap. J.* 218:148
Mezger PG, Tuffs RJ, Chini R, Kreysa E, Gemünd H-P. 1986. *Astron. Astrophys.* 167:145
Michel FC, Scowen PA, Dufour RJ, Hester JJ. 1991. *Ap. J.* 368:463
Miller JS. 1978. *Ap. J.* 220:490
Moore BD, Hester JJ, Dufour RJ. 2004. *Astron. J.* 127:3484
Mori K, Burrows DN, Hester JJ, Pavlov GG, Tsunemi H. 2004. *Ap. J.* 609:186
Mori K, Yamamoto M, Kaminishizono I, Shibata S, Burrows DN et al. 2006. 36th COSPAR Sci. Assemb., ADS, Beijing, China, CDROM #2615
Murdin P. 1995. *MNRAS* 269:89
Murdin P, Clark DH. 1981. *Nature* 294:543
Ng C-Y, Romani RW. 2004. *Ap. J.* 601:479
Ng C-Y, Romani RW. 2006, *Ap. J.* 644:445
Oort JH, Walraven T. 1956. *Bull. Astron. Inst. Neth.* 12:285
Péquignot D, Dennefeld M. 1983. *Astron. Astrophys.* 120:249
Predehl P, Schmitt JHMM. 1995. *Astron. Astrophys.* 293:889
Rees MJ, Gunn JE. 1974. *MNRAS* 167:1
Romani RW, Reach WT, Koo BC, Heiles C. 1990. *Ap. J.* 349:L51
Sankrit R, Hester JJ. 1997. *Ap. J.* 491:796
Sankrit R, Hester JJ. 2000. *Ap. J.* 535:847
Sankrit R, Hester JJ, Scowen PA, Ballester GE, Burrows CJ, et al. 1998. *Ap. J.* 504:344
Scargle JD. 1969. *Ap. J.* 156:401
Schaller EL, Fesen RA. 2002. *Ap. J.* 123:941
Schmidt GD, Angel JRP, Beaver EA. 1979. *Ap. J.* 227:106
Seward FD, Gorenstein P, Smith RK. 2006. *Ap. J.* 636:873
Seward FD, Harnden FR. 1994. *Ap. J.* 421:581
Seward FD, Tucker WH, Fesen RA. 2006. *Ap. J.* 652:1277
Shklovsky IS. 1953. *Dokl. Akad. Nauk. SSSR* 90:983
Sollerman J, Lundqvist P, Lindler D, Chevalier RA, Fransson C et al. 2000. *Ap. J.* 537:861
Spitkovsky A. 2006. *Ap. J.* 648:L51
Spitkovsky A, Arons J. 2004. *Ap. J.* 603:669
Staelin DH, Reifenstein EC. 1968. *Science* 162:148
Stone JM, Gardiner T. 2007. *Ap. J.* 671:1726
Temim T, Gehrz RD, Woodward CE, Roellig TL, Smith N, et al. 2006. *Ap. J.* 132:1610
Trimble V. 1968. *Astron. J.* 73:535
Trimble V, Woltjer L. 1971. *Ap. J.* 163:L97
Uomoto A, MacAlpine GM. 1987. *Astron. J.* 93:1511
van den Bergh S. 1970. *Ap. J.* 160:L27
van den Bergh S, Pritchet CJ. 1989. *Ap. J.* 338:L69
Velusamy T. 1984. *Nature* 308:251
Wallace BJ, Landecker TL, Kalberla PMW, Taylor AR. 1999. *Ap. J. Suppl.* 124:181
Wallace BJ, Landecker TL, Taylor AR. 1994. *Astron. Astrophys.* 286:565
Wang L, Wheeler JC. 2008. *Annu. Rev. Astron. Astrophys.* 46:433–74
Weiler KW, Panagia N. 1978. *Astron. Astrophys.* 70:419
Weisskopf MC, Hester JJ, Tennant AF, Elsnor RF, Schulz NS, et al. 2000. *Ap. J.* 536:L81
Wheeler JC, Maund JR, Shizuka A. 2007. Supernova Asymmetries, *AIP Conf. Proc.*, 937:349
Wilson AS. 1974. *MNRAS* 166:617
Wyckoff S, Murray CA. 1977. *MNRAS* 180:717

Annual Review of Astronomy and Astrophysics

Volume 46, 2008

Contents

Indexes

Errata

An online log of corrections to *Annual Review of Astronomy and Astrophysics* articles may be found at http://astro.annualreviews.org/errata.shtml